

**OGLE-IV Real-Time Transient Search**

Ł. Wyrzykowski<sup>1,2</sup>, Z. Kostrzewa-Rutkowska<sup>1</sup>, S. Kozłowski<sup>1</sup>,  
A. Udalski<sup>1</sup>, R. Poleski<sup>1,3</sup>, J. Skowron<sup>1</sup>, N. Blagorodnova<sup>2</sup>, M. Kubiak<sup>1</sup>,  
M. K. Szymański<sup>1</sup>, G. Pietrzyński<sup>1,4</sup>, I. Soszyński<sup>1</sup>, K. Ulaczyk<sup>1</sup>,  
P. Pietrukowicz<sup>1</sup>, P. Mróz<sup>1</sup>

<sup>1</sup>Warsaw University Observatory

Al. Ujazdowskie 4, 00-478 Warszawa, Poland

(lw, zkostrzewa, simkoz)@astrouw.edu.pl

<sup>2</sup>Institute of Astronomy, University of Cambridge

Madingley Road, CB3 0HA Cambridge, UK

<sup>3</sup>Department of Astronomy, Ohio State University, 140 W. 18th Ave., Columbus, OH  
43210, USA

<sup>4</sup>Universidad de Concepción, Departamento de Astronomía, Casilla 160-C, Concepción,  
Chile

*Received Month Day, Year*

**ABSTRACT**

We present the design and first results of a real-time search for transients within the 650 sq. deg. area around the Magellanic Clouds, conducted as part of the OGLE-IV project and aimed at detecting supernovae, novae and other events. The average sampling of about 4 days from September to May, yielded a detection of 238 transients in 2012/2013 and 2013/2014 seasons. The superb photometric and astrometric quality of the OGLE data allows for numerous applications of the discovered transients.

We use this sample to prepare and train a Machine Learning-based automated classifier for early light curves, which distinguishes major classes of transients with more than 80% of correct answers. Spectroscopically classified 49 supernovae Type Ia are used to construct a Hubble Diagram with statistical scatter of about 0.3 mag and fill the least populated region of the redshifts range in the Union sample. We investigate the influence of host galaxy environments on supernovae statistics and find the mean host extinction of  $A_I = 0.19 \pm 0.10$  mag and  $A_V = 0.39 \pm 0.21$  mag based on a subsample of supernovae Type Ia. We show that the positional accuracy of the survey is of the order of 0.5 pixels (0.13 arcsec) and that the OGLE-IV Transient Detection System is capable of detecting transients within the nuclei of galaxies. We present a few interesting cases of nuclear transients of unknown type.

All data on the OGLE transients are made publicly available to the astronomical community via the OGLE website.

**Key words:** *surveys, supernovae, novae, transients*

## 1. Introduction

In the last decade wide-field instruments installed on medium-sized telescopes have opened a new window in the time-domain astronomy. Hundreds of thousands of new variable stars have not only been found (*e.g.*, Bramich *et al.* 2008, Soszyński *et al.* 2013, Pietrukowicz *et al.* 2013, Drake *et al.* 2014), but also have been well studied thanks to dense photometric coverage collected over many years. For example, recently Soszyński *et al.* (2014) found an RR Lyrae-type star, which over the course of a few years, changed the mode of pulsation from double to single. Another remarkable example is a merger of a contact binary which resulted in a spectacular explosion (Tylenda *et al.* 2013).

Long-term sky monitoring programs are also detecting objects, which appear only for a short period of time, *i.e.*, transient events. Among the recent projects aiming at unbiased large scale observations of large fractions of the sky are SDSS-Stripe82 (Sako *et al.* 2011), the Catalina Real-Time Transient Survey (CRTS) (Drake *et al.* 2009), the Palomar Transient Factory (PTF) (Law *et al.* 2009) and the La Silla Quest (Hadjiyska *et al.* 2012), to name a few. In the very near future the ESA's space mission Gaia will provide all-sky detections and classification of transient objects (*e.g.*, Wyrzykowski and Hodgkin 2012, Blagorodnova *et al.* 2014).

Typically, a key focus of most of the transients surveys is on supernovae (SNe), primarily due to their cosmological applications (*e.g.*, Riess *et al.* 1998, Perlmutter *et al.* 1999, Sullivan *et al.* 2011, Campbell *et al.* 2013). More than 10,000 supernovae has been found to date, however, most of them were hard to study in detail due to lack of good quality photometry and insufficient amount of available spectroscopic follow-up. Another major difficulty is to detect and announce new discoveries as early as possible to allow prompt spectroscopic observations.

Type Ia supernovae, produced in thermonuclear explosion of a white dwarf exceeding a Chandrasekhar's critical mass, are "standardizable" candles (*e.g.*, Phillips 1993, Prieto *et al.* 2006) and are now routinely employed in low- and high-redshift studies of the distance scale of the Universe. However, the process of standardization is purely empirical and it still remains unclear which properties of the supernova, its nearest environment and the host are responsible for differences seen in the light curves and spectra of Type Ia SNe. The residuals on the Hubble Diagram are often used to study the influence of *e.g.*, mass of the host galaxy or its metallicity on the standardization process of the SNe (*e.g.*, Childress *et al.* 2013, Pan *et al.* 2014) or distribution of extinction in the hosts (Galbany *et al.* 2012).

Type II supernovae result from a core-collapse (CC) of a massive star. The range of possible scenarios in those explosions produces a large variety of different subtypes of CC supernovae. The most common class, Type IIP, characterized by a couple of months long plateau in the light curve, was shown to also be "standardizable" and was used as yet another type of distance indicators (*e.g.*, Poznanski 2009).

Wide-field and long-term observations increase the number of supernovae of

well known types, but also increase chances for detecting rare and unusual examples of supernovae. Exotic supernovae are being found in both the cores (*e.g.*, Mattila *et al.* 2012), or at the outskirts of galaxies (*e.g.*, Maguire *et al.* 2011), providing additional data for studying the environments of supernovae and their influence on the explosions. Other new types of transients are also being discovered, such as superluminous supernovae (SLSN, *e.g.*, Quimby *et al.* 2011) or tidal disruption events (TDE, *e.g.*, Gezari *et al.* 2012).

Here we present the results of the real-time transient search in the first two years of the monitoring program of about 650 sq. deg. around the Magellanic Clouds conducted within the OGLE-IV survey. The paper is organized as follows. In Section 2 we describe the OGLE-IV survey and the transient detection pipeline. Section 3 describes spectroscopic and photometric classifications of the OGLE-IV detections. In the next sections we present the applications of OGLE supernovae, studying the influence of environments of supernovae on their properties and light curves (Section 4) and deriving the Hubble Diagram (Section 5). We conclude in Section 6.

## 2. Observations and detection pipeline

### 2.1. The OGLE-IV project

The Optical Gravitational Lensing Experiment (OGLE) has started in 1992 as one of the first generation microlensing surveys (OGLE-I: 1992-1995). Since 1997 the OGLE survey started using a new 1.3 m Warsaw Telescope with a first generation camera (for technical details see Udalski *et al.* 1997). The OGLE observing facilities are located at the Las Campanas Observatory, Chile, operated by the Carnegie Institution for Science. In 2001 the first generation camera was replaced by an eight detector CCD mosaic (OGLE-III: 2001-2009, see Udalski *et al.* 2008a), and in 2010 another instrumental upgrade occurred. The newest generation 32 detector CCD mosaic replaced OGLE-III instrument, marking the start of the OGLE-IV phase. The new mosaic – one of the largest CCD cameras worldwide – covers the entire field of view of the Warsaw Telescope (1.4 square degrees). Each CCD is a  $4k \times 2k$  pixel E2V detector with  $15\mu\text{m}$  pixels, giving the 0.26 arcsec/pixel scale at the focus of the Warsaw Telescope. OGLE-IV uses only two filters, Johnson-Cousin *I*- and *V*- bands, however, vast majority of observations are carried out in the *I* filter.

OGLE has always been among the largest variability surveys providing hundreds thousands variable objects of all types and various transients. These were primarily microlensing events, found in thousands every year toward the Galactic Center, which are also used for finding extrasolar planets (*e.g.*, Udalski *et al.* 2005, Poleski *et al.* 2014) or studying the structure of the Galaxy (*e.g.*, Wyrzykowski *et al.* 2014). OGLE has also been discovering and gathering long-term photometric data for dwarf and classical novae (*e.g.*, Skowron *et al.* 2009, Mróz *et al.* 2014) and

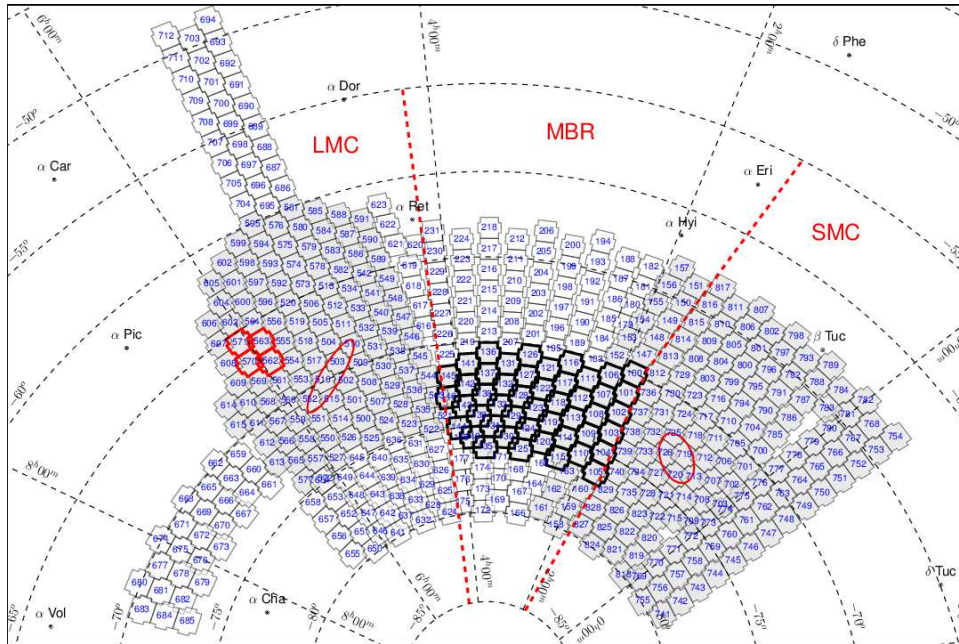


Figure 1: Map of the 475 OGLE-IV fields covering about 650 sq.deg., observed since 2010. Grey fields were used for real-time search for supernovae since October 2012 and remaining were added in June 2013. Regions are divided into LMC, MBR and SMC sections. Ellipses mark the positions of the bulk of the stars in the Large and Small Magellanic Cloud. Red-outlined fields are the Gaia SEP fields studied in Soszyński *et al.* (2012). Black-outlined are the fields searched for transients in Kozłowski *et al.* (2013).

other rare transient objects (*e.g.*, Tylenda *et al.* 2013).

Since 1994 microlensing events have been searched for in the OGLE data stream *via* the Early Warning System (EWS, Udalski *et al.* 1994, Udalski 2003). Supernovae were first searched for in the real-time OGLE data in 2003–2004 (NOOS, Udalski 2003, Udalski *et al.* 2004). However, this project was abandoned because of relatively small sky coverage during OGLE-III phase and, thus, relatively low detection rate.

The situation significantly changed in 2010 with the start of OGLE-IV when the OGLE survey commenced observations of the large area of the sky around the Magellanic Clouds. Those fields are dominated by galaxies, not stars, and thus are perfect for finding extragalactic transients. The search for transients in the archival OGLE-IV data from years 2010-2012 yielded 130 supernovae and other transients with detailed well-sampled light curves (Kozłowski *et al.* 2013). The region around the South Ecliptic Pole, used for commissioning of the Gaia satellite mission in 2014, was also searched for archival transients (Soszyński *et al.* 2012).

In October 2012 the real-time processing pipeline was prepared enabling a

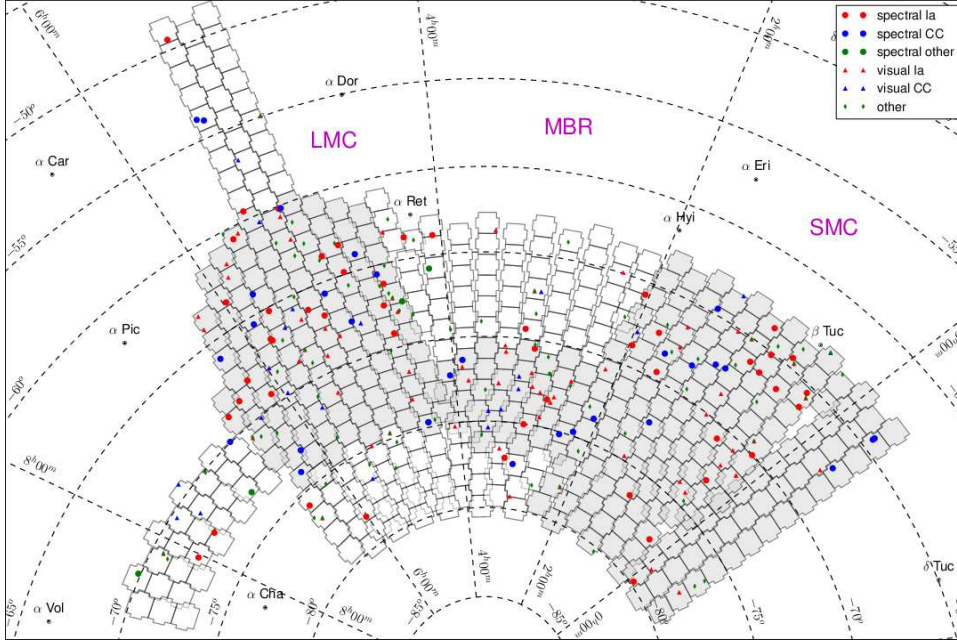


Figure 2: OGLE-IV fields as in Fig.1 displaying positions of all transients discovered in years 2012-2014. Large points show all spectroscopically observed transients, while small dots show the remaining unconfirmed objects, visually classified into classes (See text and Table 1).

search for on-going supernovae and other transients in the OGLE-IV data collected in vicinity of the Magellanic Clouds. Fig. 1 shows the map of the OGLE-IV fields observed around the Large and Small Magellanic Clouds (LMC and SMC, respectively) and the Magellanic Bridge (MBR) and Fig. 2 displays all detected transients in years 2012–2014. Most of the 475 fields have been observed regularly since 2010. 300 fields were processed in real-time since October 2012 (marked as gray in Fig. 1 and Fig. 2) and the remaining 175 were added to the pipeline in June 2013.

The observing season for the Magellanic Clouds System for the OGLE telescope runs from late July until March, *i.e.*, more than eight months, depending on the region of the System. The region around the SMC is observed for longer period of time that other regions, mostly due to lesser overlap with other OGLE programs in the Bulge and Galactic Disk. The mean cadence (Fig. 3) also varies through the season, depending of the region. The SMC and MBR sections are typically observed with frequency as high as 2 days, whereas the LMC parts can only be observed with 5 days cadence at best. Note in Fig. 3 that the overall mean cadence has degraded slightly in 2013/2014 seasons, compared to 2012/2013, due to increase in the covered area.

Fig. 4 shows in its left panel a distribution of measured seeing on individual im-

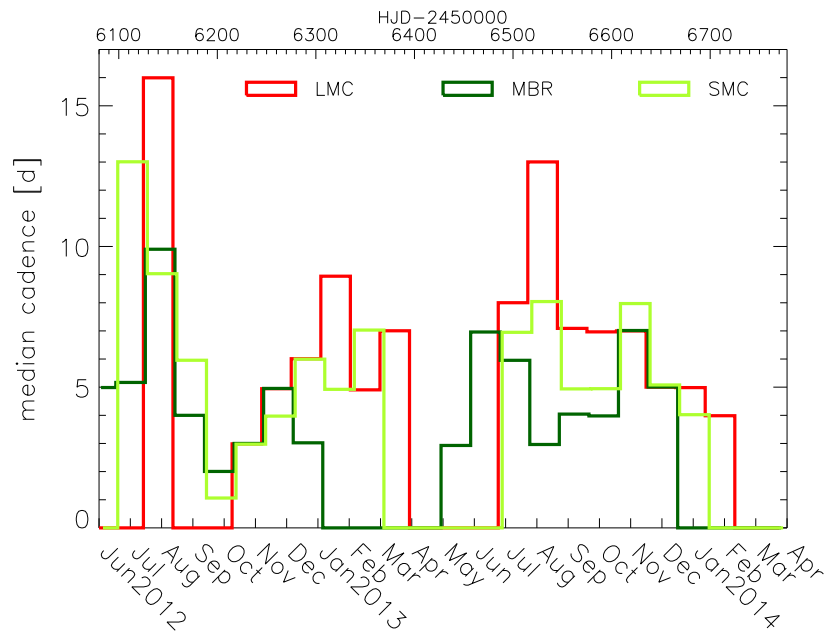


Figure 3: Mean monthly cadence between subsequent returning to the same field shown for our three observing regions. Note the cadence increase from 2 to about 4-5 days between two seasons which was caused by the increase in the number of observed fields (See the map in Fig. 1).

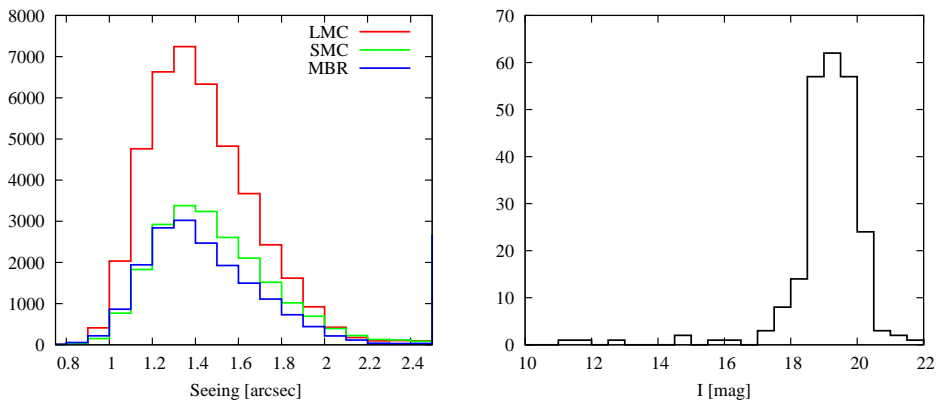


Figure 4: Left panel: distribution of seeing as measured for individual frames in seasons 2012/2013 and 2013/2014 in three different regions (LMC/MBR/SMC). The median seeing was about 1.4 arc sec for all observations. Right panel: discovery magnitude of OGLE-IV transients from seasons 2012/2013 and 2013/2014, indicating completeness by  $\sim 20$  mag in  $I$ -band.

ages used in the transient search in seasons 2012/2013 and 2013/2014. The median seeing was about 1.4 arc sec. There was a significant number of observations carried under superb seeing condition of about 1 arc second. The right panel of Fig. 4 shows a distribution of discovery magnitude of all transients detected in seasons 2012/2013 and 2013/2014. The completeness of detection reaches down to  $\sim 20$  mag, with occasional fainter detections (typically during better seeing conditions).

## 2.2. Data reductions

All the data reduction stages take place at the telescope site in near real-time. After de-biasing and flat-fielding, the data is processed by the OGLE real time photometric pipeline (Udalski 2003) which uses the Difference Imaging Analysis (DIA) technique, fine-tuned to the OGLE data and using the Woźniak (2000) implementation of Alard and Lupton (1998) algorithm. The key element in the DIA method is a set of good quality reference images, which before each subtraction are convolved to match a given image.

The static database of objects is generated prior to the real-time processing and uses reference images, which are obtained by stacking several high quality images obtained under excellent seeing conditions (better than 1 arc second). For the detection of stellar objects and determination of the reference image fluxes all the reference images were analyzed with DoPhot (Schechter *et al.* 1993), which was designed for PSF photometry of stellar objects.

In the case of a typical a few arc seconds-wide galaxy, DoPhot subdivides it into numerous smaller stellar-like objects. However, most of them are still non-PSF-like, therefore DoPhot flags them as non-stellar. For the main database only objects flagged as stars or likely stars are stored, the remaining are ignored as most of them are due to various instrumental artifacts or are caused by bright stars. Therefore, most galaxies are not in the database and the main search for transients is performed among objects not matched to template database, *i.e.*, new sources.

The search pipeline is run every day, after the data reduction of the previous night is finished, typically before Chilean noon. Then, among 475 fields we select those which were observed last night and in those data we investigate new objects, returned by the subtraction pipeline. We select those subtraction residuals which are of positive sign, *i.e.*, are caused by a brightening. The detection threshold for the brightenings is relatively high to avoid a flood of artifacts. The match to Gaussian profile of the PSF profile of brightening must exceed 0.7 (1.0 means perfect match) to classify it as a candidate new object.

In order to assure robust detections and avoid numerous cosmic rays (note, we only take one frame per field during each observing sequence), we also require that the residuals are present on at least two subsequent frames at the same location. This, therefore, naturally limits possibilities for very early detections of transients while they are still young. However, because our sampling is on average 2-5 days (see Fig. 3), our detectability time-frame is still relatively quick.

Another channel for searching for transients is conducted among objects which were there before, but changed their brightness (so called “old sources” channel). The only difference from the “new sources” channel is that the selection is made on all stars from the database which got brighter and remained so over at least two subsequent observations. We impose the upper limit on brightness at 18 mag (*i.e.*, ignore all brighter objects) in order to avoid numerous variable stars, which are typically brighter in the Magellanic Clouds.

### 2.3. Image recognition classifier

For objects selected from both “new” and “old” channels, typically about a couple thousand candidates, we generate small cutouts from the subtracted image taken at the brightest epoch. Those small imagerettes are then fed into an automated image recognition classifier. The classifier is based on a Self-Organizing Maps (SOM) technique (*e.g.*, Wyrzykowski and Belokurov 2008), trained on several thousands of small thumbnail subtraction images. The resulting SOM has  $5 \times 7$  cells and groups in each cell those imagerettes which are similar to one another, see Fig. 5. Note that most of “yin-yang” shapes are caused by genuine high proper motion of field stars, see *e.g.*, Soszyński *et al.* (2002), Poleski *et al.* (2011). After the training, the cells were visually inspected and labeled according to their thumbnail. About 30% of cells contained images of good subtractions of new stellar-like objects. The remaining were either bad subtractions, caused by misalignment of images, or effects of high proper motion of stars. The SOM classifier usually reduced the number of candidates by a factor of two, removing the most obvious and common artifacts. However, many weirdly shaped artifacts or elongated and twisted cosmic rays still remained as candidates for transients and those were removed at the final stage by visual inspection of both the images and the light curves.

We have to note here that the OGLE pipeline’s new objects selection criteria are quite stringent, requiring relatively good match to the Gaussian profile of the PSF. This results in a natural limitation on detected transients: for an image obtained under typical seeing condition of Las Campanas Observatory (about 1.2 arc seconds for the OGLE telescope), the limiting detection magnitude is about 20.0 mag in the *I*-band. For images taken with exceptionally good seeing (less than 0.9 arc seconds) the detection threshold can go down to 21 mag. However, the OGLE telescope can reach mag  $\sim 22$  in a 150 s exposure with reasonable signal-to-noise. Therefore, the second stage of the detection pipeline, which runs on manually selected candidates for transients (typically a couple per day) we perform a detailed difference imaging photometry, optimized to the known position of the transient. This allows us to obtain better quality photometry, as well as perform forced photometry of the flux of the transient when it is very faint. It also provides the timestamps of non-detection of the transient over all frames collected for that region, what allows to confirm the transient nature of the detection. Because of the data and processing limitations, we typically run the verification forced photometry of each transient on

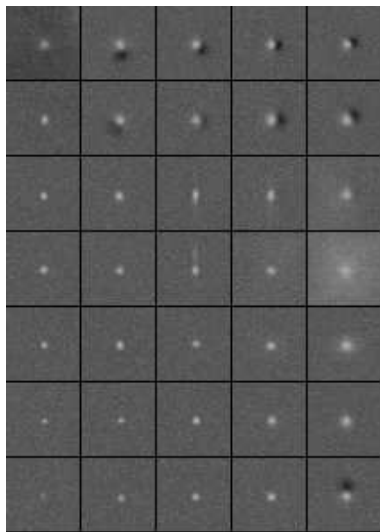


Figure 5: Visualization of nodes of the Self-Organizing Map trained on hundreds of cut-outs from the subtracted images. The map had  $5 \times 7$  nodes/cells. Yin-Yang like images and "shadows" are in most cases visible for stars with high proper motion.

frames collected within the same observing season.

Each candidate's verification photometry is then again inspected visually and we also check if there is a galaxy visible on the reference image (*i.e.*, more deep than a single frame). Additionally, we perform the cross-match with the WISE infrared catalog (Wright *et al.* 2010) in order to rule out potential transients related to the activity of the galaxy following the method of Assef *et al.* (2011) and Kozłowski *et al.* (2012) for disentangling between AGNs and galaxies. Given all the above information we make the final decision about the nature of the transient. If it is likely to be a supernova or a classical nova we give it a name following the pattern: OGLE-year-SN-number, or OGLE-year-NOVA-number, respectively. Possible dwarf nova detections or AGN activity are not reported on discovery, as they are more persistent than other transients in their nature and, moreover, can be more effectively searched for in the archival data set (*e.g.*, Kozłowski *et al.* 2011, Kozłowski *et al.* 2012, Mowlavi *et al.* 2014).

All selected on-going transients are made available to the community *via* the web-site updated more or less daily:

<http://ogle.astrouw.edu.pl/ogle4/transients/>

For each transient the photometry in the *I*- and *V*-band is provided as well as the finding chart, subtracted image and the false-color reference image. The photometry available on the real-time active web-pages is roughly calibrated to within 0.2 mag, and the calibrated light curves are obtained after the event is gone and is archived. The OGLE-IV photometry is tied to precisely calibrated OGLE Photo-

metric Maps of the Magellanic Clouds (Udalski *et al.* 2008c) based on observations collected on hundreds photometric nights. The accuracy of the zero points of OGLE-IV photometry is better than 0.02 mag.

Transients found by OGLE-IV are also announced via the Astronomers Telegram<sup>1</sup>, typically in batches once a week or less often, depending on the number of new detections.

Table 1 provides information on all OGLE-IV transients found by the Transients Detection System in real-time over the period of two seasons 2012/2013 and 2013/2014, with their basic information. The table presents all transients in order of discovery and contains the following columns: id of the transient (ID); internal OGLE-IV database id (DBID) in format *field.chip.star number*; equatorial coordinates  $RA_{J2000.0}$  and  $DEC_{J2000.0}$ ; discovery date as Julian date; discovery magnitude in *I*-band; Astronomers Telegram number with the discovery (ATEL#); photometric classification with the highest probability (phot. class., see Section 3.2); photometric classification probability (prob.); spectral type of the transient from the follow-up observations (spec.type, see Section 3.1); redshift from spectroscopic classification (*z*) or found in NED<sup>2</sup> for the nearest galaxy; ATel number with the spectroscopic classification (ATEL spec.#) or "NED" if NED redshift available only; offset in arc seconds from the nucleus of the host (see Section 4) or from the nearest galaxy found in NED (in brackets); offset from the host's center in kpc if redshift available; offset from the nucleus in units of half-light radius  $R_{Ser}$  (Offset\*, see Section 4); half-light radius of the host obtained in *galfit* model (see Section 4); classification of the nearest galaxy using WISE colors after Assef *et al.* 2010 (WISE), S=spiral, Ell=elliptical, AGN = active galactic nucleus (see Section 4); comment with visual classification type based on the entire light curve.

The data of transients found in years 2012-2014, including fully calibrated photometry and finding charts, are available in the OGLE Archive on the web-site:

<http://ogle.astrouw.edu.pl/ogle4/transients/archive2012-2014>

Kozłowski *et al.* (2013) searched for supernovae and other transients in the archival OGLE-IV data from years 2010–2012. They also provided the cumulative number of expected supernovae down to a given peak *I*-band magnitude using best available rates for most SNe types. Comparing our real-time detections to those predictions, we estimate our detection efficiency to be about 50% down to 19 mag and about 15% above 20 mag, what is naturally lower than the archival search (83% and 38%, respectively). The lower efficiency is expected, given the fact that the real-time search relies on much shorter light curves available at the time of detection, hence only the most robust objects are typically selected as transients in order to keep the sample as pure as possible.

---

<sup>1</sup><http://www.astronomerstelegam.org>

<sup>2</sup><http://ned.ipac.caltech.edu/>

ID	DBID	RA <sub>J2000.0</sub>	DEC <sub>J2000.0</sub>	Discovery HJD-2450000	Disc. I mag	ATEL #	phot. class	prob.	spec. type	z	ATEL spec.#	Offset [arcsec]	Offset [kpc]	Offset* [arcsec]	R <sub>ser</sub> [arcsec]	WISE	comment
12-NOVA-02	SMC714.19.5N	0:32:55.06	-74:20:19.7	6083.89340	11.30	-	CN	0.70	-	-	-	-	-	-	-	-	CN
12-NOVA-03	LMC500.11.11N	5:20:21.09	-73:05:43.3	6230.75237	12.93	-	CN	1.00	-	-	-	-	-	-	-	-	CN
12-SN-005	MBR126.24.184N	3:00:50.89	-70:31:11.4	6212.79171	18.62	4481	Ia	0.80	Ia	0.076	4594	4.68	6.66	5.01	2.65	S	Ia
12-SN-006	MBR134.28.15N	3:33:34.79	-74:23:40.1	6217.74826	17.61	4495	Ia	0.98	Ibn	0.06	4734	-	-	-	-	-	Ibn
12-SN-007	MBR124.11.19N	3:01:13.44	-75:01:16.1	6218.84329	18.36	4495	Ia	1.00	Ia	0.059438	4602	-	-	-	-	S	Ia
12-SN-008	LMC537.05.1N	4:33:37.01	-71:32:20.4	6137.94129	18.55	4495	CN	0.70	-	-	-	-	-	-	-	Ell	unknown likely Ia
12-SN-009	SMC700.05.8N	0:13:56.46	-70:01:41.3	6104.93091	14.89	4495	Ia	1.00	Ia	0.013966	CBET3168	(23.6)	-	-	-	-	Ia
12-SN-010	MBR122.09.9N	2:58:26.16	-72:45:12.0	6185.78812	18.23	4495	IIn	0.67	-	-	-	0.23	-	0.25	6.15	S	Ia
12-SN-011	MBR106.20.8N	2:08:45.14	-70:39:00.7	6141.86720	18.52	4495	Ia	1.00	-	-	-	5.11	-	5.23	2.64	S	Ia
12-SN-012	LMC535.26.170N	4:36:17.61	-73:09:21.9	6195.87036	18.66	4495	IIn	0.67	-	-	-	4.19	-	6.00	2.43	S	Ia
12-SN-013	LMC551.24.8N	5:42:48.70	-71:35:52.5	6185.88063	18.82	4495	IIn	0.93	-	-	-	-	-	-	-	S	IIn
12-SN-014	LMC539.06.1N	4:37:19.18	-69:08:25.2	6150.92144	18.20	4495	Ia	1.00	Ia	0.059	CBET3280	-	-	-	-	S	Ia
12-SN-015	LMC549.30.12N	4:33:19.02	-65:07:56.1	6147.94098	19.05	4495	CN	0.70	-	-	-	-	-	-	-	S	unknown
12-SN-016	LMC562.02.1N	5:58:56.36	-68:02:54.9	6158.89128	19.18	4495	CN	0.70	-	-	-	6.29	-	6.59	2.55	S	unknown likely II
12-SN-017	MBR128.21.3N	3:09:20.61	-73:00:02.6	6111.90423	19.13	4495	CN	0.70	-	0.062040	NED	10.99	-	11.39	10.36	S	IIP or III
12-SN-018	SMC717.13.18N	0:53:37.61	-70:04:01.0	6151.81165	19.13	4495	Ia	0.90	-	-	-	-	-	-	-	S	Ia
12-SN-019	MBR127.02.6N	3:09:51.27	-72:15:24.6	6160.90569	19.26	4495	Ia	1.00	-	-	-	7.77	-	11.56	12.36	S	unknown likely II
12-SN-020	SMC714.22.48N	0:27:08.75	-74:14:08.2	6140.78721	18.50	4495	DN	1.00	-	0.062293	NED	6.45	-	6.88	12.87	S	Ia
12-SN-021	MBR131.29.12N	3:21:03.26	-70:51:13.8	6159.90800	19.18	4495	Ia	0.90	-	-	-	2.77	-	3.59	3.88	S	Ia
12-SN-022	MBR133.05.7N	3:22:32.00	-74:16:34.6	6159.91212	19.76	4495	Ia	0.90	-	-	-	-	-	-	-	S	IIP
12-SN-023	LMC554.06.6N	5:40:58.11	-68:35:09.5	6181.88999	19.79	4495	Ia	1.00	-	-	-	-	-	-	-	Ell	Ia
12-SN-024	LMC532.20.243N	4:56:00.97	-68:00:31.2	6230.72111	19.49	4541	Ia	0.32	-	-	-	-	-	-	-	S	IIP
12-SN-025	MBR127.15.13N	3:00:35.50	-71:57:21.3	6191.84436	19.17	4541	Ia	1.00	-	-	-	0.12	-	0.12	0.73	S	Ia
12-SN-026	SMC705.06.76N	0:24:42.60	-70:37:07.7	6234.71349	19.21	4578	IIP	0.92	-	-	-	4.57	-	5.71	2.60	S	Ia
12-SN-027	SMC738.03.156N	1:35:11.24	-73:35:36.7	6242.72138	19.30	4578	Ia	1.00	I(maybe)	0.07	4558	-	-	-	-	S	I
12-SN-028	MBR119.09.18N	2:48:21.42	-74:26:40.0	6237.78721	19.75	4578	IIP	0.92	-	-	-	-	-	-	-	S	Ia
12-SN-029	MBR132.10.17N	3:25:33.65	-72:44:37.8	6237.81540	19.57	4578	Ia	0.79	-	-	-	0.74	-	0.83	2.08	S	Ia
12-SN-030	LMC547.20.71N	4:31:51.85	-67:56:47.9	6239.84822	18.76	4578	Ia	1.00	-	0.066509	NED	3.91	-	4.18	2.08	S	Ia
12-SN-031	LMC515.15.153N	5:27:42.45	-71:15:50.6	6243.81787	19.87	4578	Ia	1.00	-	-	-	-	-	-	-	S	Ia
12-SN-032	LMC506.02.16N	5:22:08.05	-66:09:47.2	6248.81761	18.73	4578	Ia	1.00	Ia	0.063	4602	-	-	-	-	Ell	Ia
12-SN-033	LMC555.12.119N	5:43:19.40	-67:04:21.0	6245.78759	20.09	4578	Ia	1.00	-	-	-	-	-	-	-	-	unknown
12-SN-034	LMC522.23.9N	4:21:17.75	-74:38:04.7	6246.78692	19.93	4604	IIP	0.70	-	-	-	-	-	-	-	S	unknown
12-SN-035	LMC574.23.5N	5:16:44.86	-62:59:03.5	6253.81142	19.48	4604	IIP	0.48	-	-	-	6.60	-	6.67	4.19	S	unknown
12-SN-036	LMC606.01.2N	6:15:42.01	-64:08:57.9	6247.82342	18.75	4604	IIP	0.48	-	-	-	3.77	-	7.00	4.71	S	Ia
12-SN-037	LMC611.14.4N	6:21:27.72	-70:05:48.5	6158.91761	19.56	4604	CN	0.70	-	-	-	5.07	3.59	7.73	7.05	S	unknown likely II
12-SN-038	LMC561.22.79N	5:55:53.05	-68:28:43.5	6249.76224	19.96	4604	IIP	0.70	-	-	-	8.78	-	10.35	7.21	S	unknown
12-SN-039	LMC612.20.18N	6:29:40.49	-70:55:36.0	6252.84831	20.02	4604	IIP	0.70	-	-	-	4.06	-	5.82	2.74	S	unknown
12-SN-040	LMC568.14.15N	6:07:01.59	-69:21:17.1	6264.81780	15.95	4604	Ia	1.00	Ia	0.014690	4618	0.76	0.22	0.76	3.93	Ell	Ia
12-SN-041	LMC538.10.26N	4:42:23.37	-70:05:46.3	6264.76484	19.79	4641	Ia	0.30	-	-	-	-	-	-	-	S	unknown
12-SN-042	LMC595.07.4N	5:25:27.44	-60:24:35.8	6246.76639	18.66	4641	IIn	0.67	-	-	-	7.52	-	7.52	2.71	S	unknown likely II
12-SN-043	LMC576.24.6N	5:15:38.11	-60:36:06.4	6266.82530	19.07	4641	Ia	0.99	-	-	-	-	-	-	-	S	Ia
12-SN-044	LMC576.32.362N	5:14:53.48	-60:08:47.7	6276.79792	18.42	4641	Ia	1.00	Ia	0.06	4734	-	-	-	-	S	Ia
12-SN-045	LMC580.19.9N	5:11:28.24	-61:08:29.7	6285.75809	19.66	4657	Ia	0.90	-	-	-	-	-	-	-	-	unknown
12-SN-046	LMC595.28.7N	5:29:47.99	-59:29:59.4	6277.82714	19.27	4657	Ia	0.90	Ia	0.111	4734	1.69	3.37	2.53	0.91	S	Ia
12-SN-047	MBR144.11.34N	4:04:14.25	-75:12:08.2	6263.72945	19.67	4657	Ia	0.36	-	-	-	1.16	-	1.51	0.76	S	Ia
12-SN-048	SMC732.19.38N	1:23:14.23	-72:19:54.7	6297.58574	18.37	4676	IIn	0.67	IIn	0.067	4696	3.58	4.54	3.82	3.88	S	IIn

Table 1: Properties of all transients found by the OGLE-IV Transients Detection System in seasons 2012-2014. See main text for details.

ID	DBID	RA <sub>J2000.0</sub>	DEC <sub>J2000.0</sub>	Discovery HJD-2450000	Disc. <i>I</i> mag	ATEL #	phot. class	prob.	spec. type	z	ATEL spec.#	Offset [arcsec]	Offset [kpc]	Offset* [arcsec]	<i>R</i> <sub>Ser</sub> [arcsec]	WISE	comment
12-SN-049	SMC711.14.32N	0:37:48.09	-70:44:46.5	6285.58220	18.65	4676	IIn	0.67	Ia	0.07	4696	-	-	-	-	S	Ia
12-SN-050	LMC564.04.23N	5:52:34.36	-65:26:59.7	6311.71617	18.19	4689	IIn	0.97	IIn	0.082	4696	3.56	5.43	3.58	2.04	S	IIn
12-SN-051	LMC578.24.12N	5:04:06.71	-63:34:57.0	6290.78024	19.73	4689	Ia	0.90	Ia	0.11	4698	6.32	12.52	6.90	2.22	S	Ia
12-SN-052	LMC599.23.6N	5:36:29.34	-60:28:37.5	6255.80414	18.97	4690	IIP	0.48	-	-	-	0.28	-	0.42	3.62	S	Ia
13-SN-001	SMC797.03.426N	0:46:30.44	-65:08:16.4	6297.55517	18.83	4718	IIP	0.48	Ia	0.09	4721	-	-	-	-	S	Ia
13-SN-002	SMC810.26.1800N	1:23:30.46	-64:39:42.9	6301.57563	18.52	4718	IIn	0.67	II	0.0722	4721	1.10	1.49	1.17	1.72	S	IIn
13-SN-003	SMC743.13.16N	23:15:46.39	-76:58:17.1	6263.59832	18.43	4718	Ia	0.46	-	-	-	0.09	-	0.10	3.47	S	unknown likely nuclear
13-SN-004	SMC769.06.26N	23:53:52.50	-79:46:19.0	6287.59400	18.61	4718	Ia	1.00	Ia	0.06	4734	13.20	15.11	13.89	4.62	S	Ia
13-SN-005	SMC799.18.93N	1:01:37.14	-67:18:01.7	6258.59090	19.68	4718	IIP	0.48	II	0.07	4734	-	-	-	-	S	IIP
13-SN-006	SMC800.03.333N	0:58:08.06	-66:48:26.7	6271.54521	19.44	4718	Ia	0.90	-	0.069548	NED	(24.7)	-	-	-	-	unknown
13-SN-007	SMC805.29.180N	1:07:56.84	-65:09:14.4	6290.63757	19.24	4718	IIP	0.92	-	-	-	16.64	-	16.72	5.32	-	unknown likely Ia
13-SN-008	SMC813.32.1389N	1:30:57.95	-67:39:12.4	6237.66789	18.82	4718	Ia	1.00	-	-	-	2.63	-	4.25	2.85	S	Ia
13-SN-009	LMC549.03.218N	4:36:08.21	-66:09:41.2	6296.74994	18.67	4746	Ia	1.00	Ia	0.060	4734	2.20	2.52	2.20	2.79	S	Ia
13-SN-010	MBR142.13.82N	3:49:19.65	-72:33:34.6	6309.61450	19.26	4746	IIP	0.48	-	-	-	-	-	-	-	S	Ia
13-SN-011	LMC586.12.12N	4:47:10.92	-64:02:36.5	6319.65283	18.83	4746	IIP	0.48	IIP	0.05	4754	5.00	4.82	5.04	3.07	S	IIP
13-SN-012	LMC512.27.28N	5:09:52.38	-65:39:48.6	6319.62598	19.07	-	IIn	0.93	IIn	0.08	4774	-	-	-	-	Ell	IIn
13-SN-013	MBR141.02.36N	3:53:38.01	-71:45:32.3	6309.61246	19.15	4825	Ia	1.00	-	-	-	-	-	-	-	-	Ia
13-SN-014	MBR141.11.46N	3:53:07.78	-71:20:46.6	6334.61410	17.60	4825	Ia	0.80	II	0.037	4829	1.03	0.75	1.11	2.35	S	IIP
13-SN-015	MBR155.18.157N	2:02:21.55	-65:44:08.4	6338.53517	19.38	4825	Ia	1.00	Ia	0.088	4829	-	-	-	-	S	Ia
13-SN-016	LMC581.08.1389	5:13:52.76	-60:09:26.9	6379.55018	18.68	4859	IIP	1.00	IIn	0.074	4860	-	-	-	-	AGN	IIn
13-SN-017	LMC522.21.1824	4:27:22.20	-74:42:09.4	6352.58671	18.27	4859	DN	1.00	IIn	0.043	4863	3.44	2.87	4.45	5.66	S	IIn
13-SN-018	LMC540.23.45N	4:39:13.81	-67:23:36.4	6354.57519	18.98	4875	Ia	0.36	Ia	0.067	4880	0.14	0.17	0.21	2.12	S	Ia
13-SN-019	MBR114.11.509	2:27:33.91	-75:08:16.0	6363.50225	19.48	4875	Ia	0.94	IIn	0.079	4876	-	-	-	-	S	IIP
13-SN-020	LMC575.15.23N	5:15:17.87	-62:00:44.5	6354.62311	19.51	4917	Ia	1.00	-	-	-	1.94	-	3.31	3.59	S	Ia
13-SN-021	LMC519.14.219N	5:28:01.18	-66:30:09.0	6363.54948	18.71	4917	Ia	0.90	-	-	-	-	-	-	-	Ell	Ia
13-SN-022	MBR121.29.878	2:50:17.36	-70:52:27.8	6369.51506	20.01	4917	Ia	0.98	-	-	-	3.30	-	4.55	2.65	S	unknown
13-SN-023	LMC552.07.190N	5:41:43.68	-70:56:22.7	6375.58726	19.82	4917	Ia	0.98	-	-	-	-	-	-	-	-	unknown
13-SN-024	LMC510.26.4702N	5:10:48.57	-68:16:23.8	6347.59765	19.50	4917	Ia	1.00	-	-	-	-	-	-	-	S	Ia
13-SN-025	LMC606.27.276	6:13:53.98	-63:21:25.4	6389.55255	18.80	5000	Ia	0.90	-	-	-	0.19	-	0.19	4.66	S	unknown likely Ia
13-SN-026	SMC723.10.22N	1:13:38.51	-69:32:11.4	6438.86809	19.26	5166	IIP	0.48	-	-	-	1.52	-	2.50	1.31	S	unknown
13-SN-027	SMC714.14.62N	0:22:59.80	-74:38:32.3	6459.94906	18.70	5166	IIP	0.48	-	-	-	0.14	-	0.16	1.69	S	unknown
13-SN-028	SMC789.27.52N	0:25:34.22	-62:54:52.2	6438.90375	19.73	5166	IIP	0.48	-	0.034300	NED	4.10	-	4.92	7.50	S	unknown likely II
13-SN-029	SMC714.26.7746	0:36:16.30	-73:59:57.7	6467.85673	18.77	5166	IIP	0.92	-	-	-	3.20	-	3.55	3.48	S	unknown likely Ia
13-SN-030	SMC814.30.44N	1:32:41.37	-66:25:43.3	6464.93131	18.83	5204	IIP	0.48	-	-	-	0.73	-	0.93	0.72	-	Ia
13-SN-031	SMC813.22.123	1:33:51.35	-68:07:57.5	6464.92926	19.68	5204	CN	0.70	-	-	-	-	-	-	-	S	unknown
13-SN-032	SMC787.30.67N	0:19:17.49	-65:24:42.6	6480.93958	19.26	5204	Ia	0.90	Ia	0.09	5233	10.20	16.91	10.50	2.80	S	Ia
13-SN-033	SMC743.30.2N	23:16:01.84	-76:21:09.9	6474.90090	19.07	5204	IIP	0.45	-	-	-	0.17	-	0.18	4.14	S	unknown nuclear
13-SN-034	SMC702.29.613	0:10:47.75	-71:28:28.2	6482.92392	19.68	5204	Ia	0.90	-	-	-	1.62	-	1.78	7.90	S	Ia
13-SN-035	MBR153.24.65N	1:58:24.30	-67:55:54.5	6479.95207	18.91	5220	IIP	0.48	-	-	-	0.91	-	1.84	2.45	S	unknown likely II
13-SN-036	SMC716.22.274N	0:54:27.93	-68:37:30.7	6483.85725	19.08	5220	Ia	0.36	-	-	-	1.76	-	2.25	2.33	S	Ia
13-SN-037	SMC808.14.42N	1:18:00.44	-67:43:16.3	6487.90527	19.88	5220	IIn	0.53	-	-	-	0.09	-	0.12	1.84	S	AGN-flare
13-SN-038	SMC751.09.55N	23:39:24.77	-67:02:54.8	6494.70677	17.97	5235	IIn	0.67	II	0.045	5249	-	-	-	-	S	unknown
13-SN-039	SMC707.04.24N	0:22:33.02	-72:53:41.9	6494.76434	18.94	5235	Ia	0.90	Ia	0.08	5233	2.22	3.31	3.10	3.47	S	Ia
13-SN-040	SMC802.23.63N	0:53:49.35	-63:49:24.1	6508.81760	19.25	5251	Ia	0.80	Ia	0.09	5250	1.22	2.03	1.49	1.41	S	Ia
13-SN-041	SMC812.13.110N	1:36:17.96	-69:34:12.5	6508.83856	19.44	5251	Ia	1.00	Ia	0.10	5250	2.39	4.36	2.42	3.35	S	Ia
13-SN-042	SMC706.06.7602	0:23:16.85	-71:42:49.2	6507.85177	19.82	5251	Ia	1.00	-	-	-	0.69	-	0.69	1.37	S	Ia

Table 2: Properties of all transients found by the OGLE-IV Transients Detection System in seasons 2012-2014. See main text for details.

ID	DBID	RA <sub>J2000.0</sub>	DEC <sub>J2000.0</sub>	Discovery HJD-2450000	Disc. I mag	ATEL #	phot. class	prob.	spec. type	z	ATEL spec.#	Offset [arcsec]	Offset [kpc]	Offset* [arcsec]	R <sub>Ser</sub> [arcsec]	WISE	comment	
13-SN-043	SMC800.23.1047	0:52:48.79	-66:09:48.6	6508.81269	20.27	5251	IIP	0.70	Ia	0.14	5290	2.29	5.60	2.49	2.02	S	Ia	
13-SN-044	SMC820.14.61N	0:18:50.31	-77:33:32.6	6511.78989	18.75	5277	Ia	0.90	Ia	0.07	5284	0.99	1.31	1.03	1.75	S	Ia	
13-SN-045	SMC753.19.44N	23:40:36.52	-64:17:22.6	6515.81102	20.03	5277	IIP	0.70	II	0.10	5290	-	-	-	-	-	IIP	
13-SN-046	SMC804.05.88N	1:07:29.73	-67:26:03.6	6514.80302	19.66	5277	Ia	0.90	II	0.07	5290	-	-	-	-	S	IIP	
13-SN-047	SMC753.19.43N	23:40:35.48	-64:24:22.7	6515.81102	18.35	5277	Ia	1.00	II	0.06	5284	1.40	1.60	1.86	2.61	-	IIP	
13-SN-048	SMC813.11.50N	1:37:10.25	-68:23:48.6	6519.75978	19.77	5292	IIin	0.53	II	0.06	5290	1.75	2.00	2.89	1.94	S	IIP	
13-SN-049	MBR138.13.114N	3:36:04.02	-73:09:11.5	6519.86362	18.51	5292	IIin	0.67	-	-	-	-	-	-	-	S	AGN-flare	
13-SN-050	SMC793.20.1N	0:36:11.73	-63:45:36.5	6520.71662	19.00	5292	Ia	0.32	unkn	0.13	5338	0.09	0.22	0.10	2.95	S	GalaxyAGN	
13-SN-051	SMC791.12.33N	0:32:19.55	-66:25:44.3	6520.71233	18.73	5292	Ia	0.90	Ia	0.07	5335	1.80	2.38	1.81	1.98	S	Ia	
13-SN-052	MBR118.20.216N	2:39:53.91	-73:07:05.3	6520.87379	19.48	5292	Ia	1.00	-	-	-	12.29	-	17.29	5.32	S	Ia	
13-SN-053	MBR117.15.46N	2:29:49.33	-71:57:45.2	6520.87173	19.18	5321	Ia	1.00	-	-	-	0.89	-	1.77	2.98	S	Ia	
13-SN-054	MBR122.04.597	2:51:33.57	-73:00:49.3	6521.77577	19.83	5321	Ia	1.00	-	-	-	0.86	-	0.86	1.44	S	Ia	
13-SN-055	SMC702.29.613	0:10:47.75	-71:28:28.2	0.00000	19.68	5321	Ia	0.90	-	-	-	-	-	-	-	S	Ia	
13-SN-056	LMC583.23.313	4:55:34.55	-63:05:31.2	6522.93175	20.44	5321	Ia	0.94	-	-	-	0.13	-	0.16	1.54	S	unknown	
13-SN-057	SMC793.02.42N	0:37:02.41	-64:29:50.0	6531.83447	19.40	5368	IIP	0.48	Ia	0.10	5345	1.25	2.28	1.28	1.45	S	Ia	
13-SN-058	MBR200.11.30N	2:51:13.59	-63:59:33.8	6531.88532	17.61	5368	CN	0.70	-	-	-	7.11	-	8.98	4.01	S	unknown-likelyIIin	
13-SN-059	MBR202.13.2N	3:03:11.21	-68:27:39.8	6526.81470	18.72	5368	IIP	0.45	-	-	-	-	-	-	-	S	AGN	
13-SN-060	LMC602.04.31N	5:48:11.18	-61:42:15.4	6538.90401	18.63	5368	Ia	0.80	-	-	-	-	-	-	-	S	Ia	
13-SN-061	LMC575.18.398	5:22:33.54	-61:53:54.8	6533.89871	19.96	5368	IIin	0.53	-	-	-	1.23	-	1.36	5.78	S	unknown	
13-SN-062	LMC601.20.1216	5:50:53.43	-62:24:43.8	6538.90194	19.26	5368	Ia	0.36	-	-	-	0.29	-	0.30	1.14	S	Ia	
13-SN-063	MBR203.14.488	3:01:54.01	-67:07:49.6	6537.86792	19.63	5368	IIP	0.48	-	-	-	-	-	-	-	-	IIP	
13-SN-064	MBR207.03.928	3:21:53.46	-70:29:46.1	6537.87613	18.48	5368	IIin	0.67	-	-	-	2.99	-	3.00	3.27	S	Ia	
13-SN-065	SMC824.07.741	0:56:40.86	-80:16:33.3	6537.80629	19.68	5368	IIP	0.48	-	-	-	0.47	-	0.49	1.17	S	unknown	
13-SN-066	LMC622.22.4N	4:26:10.28	-62:31:07.0	6543.92258	17.66	5397	Ia	0.80	-	0.017509	NED	0.22	-	0.24	3.91	S	AGN	
13-SN-067	MBR135.28.39N	3:39:46.50	-75:47:33.6	6545.81138	19.83	5397	IIin	0.53	-	-	-	7.62	-	7.95	8.51	S	unknown-likelyIIP	
13-SN-068	LMC517.03.1385N	5:34:00.16	-69:03:06.1	6547.87983	19.12	5397	Ia	0.36	-	-	-	-	-	-	-	S	unknown-likelyIIin	
13-SN-069	SMC811.31.1104N	1:15:50.70	-63:17:17.3	6543.82157	19.97	5397	IIin	0.53	-	-	-	-	-	-	-	S	IIP	
13-SN-070	SMC796.04.44N	0:45:14.41	-66:19:50.6	6545.75057	17.89	5397	Ia	1.00	Ia	0.043	5455	-	-	-	-	-	Ia	
13-NOVA-01	MBR220.01.13N	3:55:06.25	-69:23:40.9	6523.83008	14.69	-	CN	1.00	-	-	-	-	-	-	-	-	CN	
13-SN-071	LMC520.15.10585	5:26:09.30	-65:08:13.4	6548.86404	19.13	5397	IIP	0.48	-	-	-	0.21	-	0.23	7.34	S	unknown	
13-SN-072	MBR226.15.30N	3:59:37.66	-69:29:26.6	6546.86585	19.32	5445	IIP	1.00	-	-	-	0.31	-	0.33	7.10	AGN	AGN-flare	
13-SN-073	MBR118.09.63N	2:44:54.81	-73:20:35.8	6564.71252	19.05	5445	Ia	0.90	Ia	0.091	5400	4.46	7.47	4.69	5.29	S	Ia	
13-SN-074	MBR121.06.54N	2:47:14.24	-71:49:32.0	6563.74401	18.77	5445	IIP	0.48	-	-	-	2.56	-	5.71	6.67	S	unknown	
13-SN-075	MBR153.07.76N	1:58:01.88	-68:45:47.9	6565.85535	18.95	5445	Ia	0.90	Ia	0.08	5440	4.67	6.97	6.02	4.55	S	Ia	
13-SN-076	LMC555.32.3252N	5:38:31.91	-66:29:38.9	6561.85555	18.02	5445	IIin	0.97	-	-	-	-	-	-	-	S	IIin	
13-SN-077	MBR179.21.47N	2:08:49.55	-67:22:50.5	6563.75965	20.58	5445	IIP	0.42	-	-	-	-	-	-	-	-	unknown	
13-SN-078	SMC739.06.52N	1:26:31.49	-74:44:53.1	6565.66621	19.12	5445	DN	1.00	-	-	-	3.79	-	3.80	2.76	AGN	Ia	
13-SN-079	SMC790.09.68N	0:35:10.20	-67:41:08.5	6565.68692	19.81	5445	Ia	1.00	I	0	5443	-	-	-	-	S	unknown	
13-SN-080	SMC735.14.52N	1:02:33.24	-76:27:24.2	6565.65763	19.60	5445	Ia	0.99	Ia	0.103	5443	3.80	7.11	3.95	2.36	S	Ia	
13-SN-081	LMC677.06.13N	8:11:38.05	-70:57:43.5	6562.88325	18.90	5455	-	-	-	-	-	-	-	-	-	-	S	-
13-SN-082	LMC549.01.26N	4:38:39.51	-66:13:58.2	6567.89397	18.55	5488	IIin	0.67	-	0.048867	NED	-	-	-	-	S	AGN-flare	
13-SN-083	MBR110.12.51N	2:05:48.86	-75:42:26.2	6569.74423	20.37	5488	IIP	0.45	-	-	-	-	-	-	-	S	unknown	
13-SN-084	MBR118.02.78N	2:41:49.12	-73:27:52.5	6569.76567	19.71	5488	IIP	1.00	-	-	-	7.08	-	7.12	5.03	S	Ia	
13-SN-085	MBR187.22.207N	2:18:14.52	-64:56:59.6	6568.83820	19.25	5488	Ia	1.00	-	-	-	0.57	-	0.66	3.16	S	Ia	
13-SN-086	SMC797.20.360N	0:46:36.36	-64:31:06.7	6569.69769	20.35	5488	Ia	0.97	-	-	-	5.33	-	5.42	7.01	S	unknown	
13-SN-087	LMC534.12.38N	4:55:44.52	-65:40:27.8	6571.87145	19.71	5488	Ia	0.36	-	-	-	4.62	-	5.52	1.70	Ell	unknown	

Table 3: Properties of all transients found by the OGLE-IV Transients Detection System in seasons 2012-2014. See main text for details.

ID	DBID	RA <sub>J2000.0</sub>	DEC <sub>J2000.0</sub>	Discovery HJD-2450000	Disc. I mag	ATEL #	phot. class	prob.	spec. type	z	ATEL spec.#	Offset [arcsec]	Offset [kpc]	Offset* [arcsec]	R <sub>Ser</sub> [arcsec]	WISE	comment
13-SN-088	LMC548.07.41N	4:27:44.75	-67:24:22.4	6573.79563	19.59	5488	IIP	0.48	AGN	0.168	5459	-	-	-	-	AGN	AGN
13-SN-089	LMC599.26.1289N	5:42:37.14	-60:09:12.2	6572.84328	19.47	5488	IIP	0.48	-	-	-	6.36	-	6.71	5.13	S	unknown
13-SN-090	MBR229.10.1N	4:08:38.82	-65:45:59.2	6571.75868	18.64	5488	Ia	0.80	AGN	0.125	5537	0.10	0.23	0.11	5.45	AGN	AGN
13-SN-091	LMC596.26.1733N	5:44:44.23	-63:55:51.1	6575.87438	18.51	5488	Ia	0.80	Ic	0.08	5510	6.32	9.42	7.67	9.22	Ell	Ic
13-SN-092	SMC742.20.305N	23:17:21.63	-77:53:55.5	6572.62264	20.13	5488	Ia	1.00	-	-	-	-	-	-	-	-	Ia
13-SN-093	LMC503.19.415N	5:23:09.14	-69:03:46.2	6571.84517	19.81	5488	Ia	0.36	-	-	-	-	-	-	-	S	Ia
13-SN-094	LMC644.05.41N	5:34:48.25	-76:38:39.8	6573.80699	19.52	5488	Ia	1.00	-	-	-	0.47	-	0.52	1.10	S	unknown
13-NOVA-02	LMC649.28.33N	5:57:58.35	-74:54:08.9	6771.49064	11.55	-	CN	0.90	-	-	-	-	-	-	-	-	CN
13-SN-095	LMC657.18.66N	6:43:01.30	-76:25:11.2	6584.87665	18.77	5497	DN	1.00	-	-	-	-	-	-	-	S	DN
13-SN-096	LMC599.20.159N	5:39:38.80	-60:39:32.1	6584.78940	19.60	5497	Ia	0.90	Ia	0.11	5510	5.89	11.68	8.01	4.60	S	Ia
13-SN-097	LMC548.19.44N	4:34:33.92	-66:46:42.7	6584.83860	19.77	5497	Ia	0.90	-	-	-	1.87	-	2.54	14.39	S	unknown
13-SN-098	LMC712.04.7N	5:26:36.40	-49:28:03.9	6583.86939	18.70	5497	Ia	0.90	Ia	0.06	5504	1.15	1.32	1.50	3.99	S	Ia
13-SN-099	LMC676.12.15N	8:02:27.32	-72:25:26.6	6585.87341	17.71	5497	Ia	1.00	Ia	0.028	550	3.71	2.06	4.35	7.84	S	Ia
13-SN-100	MBR114.24.1106	2:16:18.56	-74:45:23.7	6586.67071	18.89	5497	IIP	0.48	II-pec	0.09	5617	1.05	1.74	1.11	2.57	S	unknown-peculiar
13-SN-101	LMC579.20.639	5:10:10.57	-62:31:29.2	6584.76180	19.84	5497	IIP	0.70	-	-	-	2.29	-	2.90	3.78	S	unknown
13-SN-102	LMC644.24.2119	5:31:12.75	-75:50:49.6	6584.84950	19.11	5497	IIP	0.70	-	-	-	0.00	-	0.01	0.44	-	unknown-likely DN
13-SN-103	MBR121.06.808	2:46:12.84	-71:50:45.0	6585.75997	18.71	5497	IIP	0.48	-	-	-	2.10	-	2.48	2.53	S	unknown/I/IIb
13-SN-104	MBR171.22.812	3:22:00.48	-76:34:11.6	6586.69717	19.15	5497	Ia	1.00	-	-	-	0.19	-	0.21	2.24	S	Ia
13-SN-105	MBR213.27.331	3:38:44.20	-69:06:01.4	6585.77689	19.80	5497	Ia	0.90	-	0.051479	NED	14.89	-	14.92	9.04	S	unknown
13-SN-106	SMC770.06.363	23:53:06.84	-78:33:19.5	6583.58641	19.30	5497	Ia	0.98	-	-	-	1.20	-	1.44	2.20	S	Ia
13-SN-107	SMC787.23.110N	0:17:38.87	-65:39:34.8	6595.60489	19.84	5535	Ia	1.00	-	-	-	-	-	-	-	-	Ia
13-SN-108	SMC784.27.66N	0:14:10.58	-63:19:31.2	6595.59871	18.90	5535	IIin	0.42	-	-	-	0.46	-	0.46	2.26	S	unknown
13-SN-109	MBR148.22.532N	1:46:09.34	-67:28:00.1	6595.66504	19.22	5535	Ia	0.99	Ia	0.088	5537	3.70	6.02	3.71	12.70	S	Ia
13-SN-110	SMC801.19.64N	0:59:40.13	-65:04:57.2	6600.60124	18.84	5581	Ia	0.90	-	-	-	(2.1)	-	-	-	-	Ia
13-SN-111	SMC765.15.1578	23:42:18.27	-67:39:38.8	6604.52732	19.78	5581	Ia	1.00	-	-	-	1.04	-	2.34	3.52	S	Ia
13-SN-112	LMC519.30.237N	5:29:47.48	-65:44:13.7	6608.84498	19.00	5581	IIP	0.48	-	-	-	-	-	-	-	S	IIin
13-SN-113	LMC550.07.4184	5:44:32.80	-73:32:08.1	6607.80106	19.96	5581	IIP	0.70	-	-	-	0.60	-	1.10	1.31	S	unknown
13-SN-114	SMC700.19.63N	0:19:35.61	-69:24:12.5	6609.51537	19.45	5581	Ia	0.99	-	-	-	2.29	-	2.65	3.51	S	Ia
13-SN-115	MBR126.32.2978N	3:00:56.46	-70:16:47.9	6610.68031	19.78	5581	IIP	0.53	-	-	-	-	-	-	-	S	unknown
13-SN-116	MBR167.02.21N	3:05:37.43	-79:16:57.8	6610.63029	19.07	5581	Ia	0.32	-	-	-	2.01	-	2.02	3.82	Ell	Ia
13-SN-117	LMC640.28.6330	5:21:53.08	-74:55:42.7	6614.83575	18.12	5608	IIin	0.67	-	-	-	1.16	-	1.43	2.42	S	Ia
13-SN-118	LMC505.24.64N	5:14:47.50	-66:50:29.1	6617.72346	19.01	5608	Ia	1.00	Ia	0.07	5595	6.18	8.16	6.81	2.75	S	Ia
13-SN-119	LMC566.28.27N	6:19:45.55	-71:20:19.4	6617.73597	19.98	5608	IIP	0.42	-	-	-	-	-	-	-	Ell	DN
13-SN-120	LMC556.29.2646	5:41:49.26	-65:13:05.4	6618.81650	18.95	5608	Ia	0.90	Ia	0.07	5595	-	-	-	-	S	Ia
13-SN-121	LMC616.26.2478	4:22:42.87	-68:16:34.2	6618.72813	21.17	5608	IIP	0.42	-	-	-	9.21	-	9.25	7.24	S	unknown
13-SN-122	LMC620.21.311	4:14:53.34	-63:58:35.1	6618.73757	21.16	5608	IIP	0.70	-	-	-	0.04	-	0.04	1.22	S	unknown
13-SN-123	LMC604.05.69N	5:58:30.38	-63:33:38.3	6616.78872	18.36	5608	IIin	0.67	Ia	0.08	5602	0.16	0.23	0.16	1.99	Ell	Ia
13-SN-124	MBR201.19.51N	3:08:52.84	-69:25:09.7	6622.68027	20.22	5608	Ia	0.90	Ia	0.13	5615	(29.6)	-	-	-	-	Ia
13-SN-125	LMC621.26.1477N	4:30:02.84	-63:11:29.9	6622.74714	19.94	5608	Ia	0.90	-	-	-	12.53	-	12.53	2.75	S	Ia
13-SN-126	LMC620.18.111N	4:19:47.17	-63:43:21.6	6622.74502	19.15	5608	Ia	1.00	Ia	0.06	5615	-	-	-	-	-	Ia
13-SN-127	MBR203.11.294	3:05:57.62	-67:08:18.5	6622.68470	20.74	5608	Ia	0.94	-	-	-	1.02	-	1.02	1.41	S	Ia
13-SN-128	LMC636.05.3425	4:59:42.75	-75:18:04.8	6623.79520	19.24	5608	IIP	0.48	-	-	-	2.09	-	2.45	3.95	S	unknown/IIP
13-SN-129	SMC787.06.77N	0:16:41.97	-66:16:07.4	6625.56369	19.45	5663	Ia	0.99	Ia	0.08	5622	11.54	17.20	11.81	4.92	S	Ia
13-SN-130	LMC615.28.29N	6:36:46.99	-68:52:22.4	6627.85385	19.65	5663	IIP	0.48	Ia-pec	0.09	5620	-	-	-	-	S	Ia-pec
13-SN-131	MBR149.05.146N	1:43:36.96	-66:50:39.7	6629.62253	19.48	5663	Ia	0.90	-	-	-	4.03	4.62	5.82	4.82	S	unknown
13-SN-132	LMC612.26.1546N	6:34:30.72	-70:40:00.3	6635.81133	19.69	5663	Ia	1.00	-	-	-	5.53	-	5.54	3.45	S	Ia

Table 4: Properties of all transients found by the OGLE-IV Transients Detection System in seasons 2012-2014. See main text for details.

ID	DBID	RA <sub>J2000.0</sub>	DEC <sub>J2000.0</sub>	Discovery HJD-2450000	Disc. I mag	ATEL #	phot. class	prob.	spec. type	z	ATEL spec.#	Offset [kpc]	Offset [arcsec]	Offset* [arcsec]	R <sub>ser</sub> [arcsec]	WISE	comment
13-SN-133	LMC560.22.309N	5:57:43.83	-69:50:06.2	6636.81928	19.43	5663	IIP	0.90	-	-	-	-	-	-	-	S	IIP
13-SN-134	LMC565.24.54N	6:13:58.04	-72:58:24.9	6636.81237	18.85	5663	Ia	0.90	Ic-pec	0.039	5696	-	-	-	-	S	Ic-pec
13-SN-135	MBR168.20.211N	3:06:48.20	-77:24:28.4	6636.60643	19.22	5663	IIP	0.92	II	0.057	5718	3.46	3.77	3.52	3.08	S	IIP
13-SN-136	LMC582.05.55N	4:55:46.85	-64:51:20.4	6639.75154	19.33	5663	Ia	1.00	Ia	0.080	5696	4.42	6.60	10.70	8.99	S	Ia
13-SN-137	MBR108.05.107N	2:03:34.72	-73:36:22.7	6639.60394	19.14	5663	IIP	0.48	IIIn	0.075	5686	5.85	8.23	6.73	6.49	S	IIIn
13-SN-138	SMC729.32.3036N	1:19:02.87	-68:13:14.7	6638.56148	18.59	5663	IIIn	0.94	IIIn	0.115	5683	-	-	-	-	S	IIIn
13-SN-139	LMC677.15.55N	8:09:25.36	-70:37:59.3	6640.84276	20.07	5663	Ia	1.00	-	-	-	3.38	-	3.39	2.26	S	Ia
13-SN-140	LMC636.21.5988	5:02:52.42	-74:40:11.3	6639.71997	20.20	5663	IIP	0.70	-	-	-	0.01	-	0.01	0.43	-	Ia
13-NOVA-03	MBR115.04.1856	2:26:43.16	-76:34:37.8	6637.60535	17.15	-	CN	0.80	-	-	-	-	-	-	-	-	CN
13-SN-141	MBR171.15.67	3:16:00.60	-77:05:38.5	6640.62861	18.96	5663	Ia	0.90	Ia	0.05	5696	0.09	0.08	0.23	5.05	S	Ia
13-SN-142	MBR162.24.72N	2:10:37.64	-78:01:50.2	6640.58723	19.34	5697	Ia	0.90	-	-	-	3.87	-	4.58	4.62	S	Ia
13-SN-143	LMC657.11.2388	6:37:30.46	-76:45:00.1	6645.76906	20.56	5697	Ia	0.88	-	-	-	1.60	-	1.63	1.80	S	Ia
13-SN-144	LMC511.15.104N	5:00:57.18	-67:44:25.7	6647.74442	18.76	5697	Ia	1.00	II	0.04	5696	-	-	-	-	S	IIP/IIIL
13-SN-145	LMC547.20.284N	4:30:38.05	-67:54:31.2	6647.70245	19.80	5697	Ia	0.80	-	-	-	9.17	-	9.22	3.50	S	unknown
13-SN-146	LMC548.11.58N	4:33:00.74	-67:05:21.5	6647.70467	18.69	5697	Ia	1.00	-	-	-	-	-	-	-	S	Ia
13-SN-147	LMC563.07.67N	5:48:57.86	-66:40:15.7	6649.78517	19.06	5697	IIP	0.48	Ia-pec	0.099	5689	0.08	0.14	0.09	6.57	S	Ia-pec
13-SN-148	LMC658.10.39N	6:38:06.94	-75:43:36.6	6652.70473	19.78	5697	Ia	1.00	Ia	0.043	5701	-	-	-	-	S	Ia
13-SN-149	LMC708.12.33N	5:27:36.13	-54:04:25.2	6653.59944	20.02	5709	Ia	1.00	II	0.079	5720	6.34	9.34	6.38	4.58	S	IIIn
13-SN-150	LMC504.30.333N	5:17:28.40	-67:33:29.7	6654.76446	20.15	5709	Ia	0.90	-	-	-	-	-	-	-	Ell	Ia
13-SN-151	LMC517.28.304N	5:34:24.69	-68:10:07.8	6654.77073	20.08	5709	IIP	0.92	-	-	-	-	-	-	-	S	Ia
13-SN-152	MBR134.03.729N	3:33:38.89	-75:21:16.8	6656.64804	19.20	5709	Ia	0.90	-	-	-	-	-	-	-	S	IIP
13-SN-153	SMC792.28.83N	0:34:37.69	-64:42:10.1	6656.53603	18.75	5709	Ia	1.00	-	-	-	2.43	-	3.61	3.21	S	Ia
13-SN-154	LMC654.04.36N	6:14:28.06	-75:23:53.3	6657.67448	20.49	5709	IIIn	0.51	-	-	-	0.13	-	0.13	1.11	S	unknown
13-SN-155	LMC669.10.39N	7:35:27.88	-71:15:07.1	6657.84450	20.45	5709	Ia	0.71	-	-	-	2.38	-	2.40	2.06	-	IIP or IIIn
13-SN-156	LMC583.15.1914	4:54:08.66	-63:15:37.1	6657.80890	20.31	5709	Ia	0.90	Ia	0.14	5716	0.03	0.08	0.07	1.73	S	Ia
14-SN-001	LMC664.05.78N	7:02:35.58	-72:48:15.9	6659.75454	19.07	5817	Ia	0.32	CV	0	5718	-	-	-	-	S	DN
14-SN-002	MBR231.04.42N	4:04:31.71	-63:50:15.6	6660.72357	19.53	5817	Ia	0.90	Ia	0.10	5748	2.75	5.01	3.34	4.90	S	Ia
14-SN-003	MBR108.19.69N	2:09:59.06	-73:02:11.8	6664.62577	19.10	5817	IIP	0.48	-	-	-	3.23	-	3.73	2.34	S	unknown
14-SN-004	LMC549.18.139N	4:38:36.94	-65:31:29.8	6668.76158	18.79	5817	IIP	0.92	IIP	0.03	5912	6.08	3.60	6.12	6.28	S	IIP
14-SN-005	LMC665.32.967	7:12:06.72	-70:07:13.2	6682.73417	21.60	5817	Ia	0.97	-	-	-	0.21	-	0.25	6.82	S	unknown
14-SN-006	LMC671.21.46N	7:45:41.68	-70:18:58.4	6682.74720	19.87	5817	IIP	1.00	-	-	-	0.07	-	0.10	1.84	S	IIP
14-SN-007	MBR117.07.95N	2:29:31.88	-72:14:03.7	6690.54118	19.04	5875	Ia	0.99	-	-	-	(1.8)	-	-	-	-	unknown
14-SN-008	LMC578.23.56N	5:05:52.96	-63:44:54.4	6693.70282	19.52	5875	Ia	1.00	-	-	-	10.59	-	10.63	3.75	AGN	unknown
14-SN-009	LMC708.18.143N	5:29:53.65	-53:53:16.6	6694.74193	19.57	5875	Ia	1.00	II	0.056	5864	1.46	1.57	1.55	6.28	S	unknown
14-SN-010	LMC614.07.2860	6:25:23.80	-68:34:20.3	6694.77028	18.95	5875	Ia	1.00	Ia	0.081	5864	0.08	0.12	0.08	0.99	-	Ia
14-SN-011	LMC659.30.53N	6:46:58.87	-69:57:24.8	6695.72994	19.89	5875	IIP	0.70	IIIn	0.083	5908	0.81	1.25	1.34	1.72	S	IIIn
14-SN-012	LMC668.31.940N	7:27:43.39	-69:20:35.0	6695.74927	20.24	5875	IIIn	0.51	-	-	-	-	-	-	-	-	unknown/IIP
14-SN-013	LMC673.32.2006N	7:40:35.37	-72:28:17.1	6695.76024	20.17	5875	Ia	1.00	-	-	-	-	-	-	-	-	Ia
14-SN-014	LMC522.21.92N	4:27:23.75	-74:42:11.1	6698.66286	18.91	5875	IIP	0.90	Ib	0.05	5891	6.17	5.96	6.43	5.60	S	Ib-unknown
14-SN-015	LMC610.19.3006	6:25:23.80	-68:34:20.3	6700.70514	18.98	5916	Ia	1.00	-	-	-	-	-	-	-	-	Ia
14-SN-016	LMC673.31.1107N	7:42:01.43	-72:29:41.4	6706.74447	19.41	5916	Ia	1.00	Ia	0.07	5908	-	-	-	-	S	Ia
14-SN-017	MBR218.07.74N	3:30:32.38	-63:43:16.1	6709.61149	19.07	5916	Ia	1.00	-	-	-	-	-	-	-	AGN	Ia
14-SN-018	LMC608.19.61N	6:18:20.35	-66:01:08.0	6710.70753	18.37	5916	IIIn	0.67	II	0.03	5915	-	-	-	-	S	IIP
14-SN-019	LMC609.07.75N	6:13:48.04	-67:55:15.0	6710.70958	17.41	5916	Ia	1.00	Ia	0.04	5915	0.52	0.41	0.67	7.41	Ell	Ia
14-SN-020	LMC577.21.2359	6:24:30.22	-73:58:10.6	6710.63295	20.27	5916	IIP	0.70	II	0.076	5934	0.04	0.06	0.09	0.82	S	IIP
14-SN-021	LMC555.18.230N	5:48:23.49	-66:47:29.7	6712.66078	17.92	5916	Ia	1.00	Ia	0.039	5919	2.80	2.14	3.20	2.21	S	Ia

Table 5: Properties of all transients found by the OGLE-IV Transients Detection System in seasons 2012-2014. See main text for details.

ID	DBID	RA <sub>J2000.0</sub>	DEC <sub>J2000.0</sub>	Discovery HJD-2450000	Disc. <i>I</i> mag	ATEL #	phot. class	prob.	spec. type	z	ATEL spec.#	Offset [arcsec]	Offset [kpc]	Offset* [arcsec]	$R_{Ser}$ [arcsec]	WISE	comment
14-SN-022	MBR145.13.195N	4:03:27.76	-72:11:27.0	6728.57155	17.10	-	IIn	0.67	IIn	0.024	5934	7.13	3.40	7.38	4.83	S	IIn
14-SN-023	LMC680.22.414N	8:26:16.27	-69:52:21.5	6715.73155	18.98	-	DN	1.00	CV	0	5937	-	-	-	-	-	DN
14-SN-024	LMC647.02.50N	6:01:15.38	-78:18:21.7	6719.64051	19.69	-	IIP	0.48	Ia	0.1	5938	-	-	-	-	S	Ia
14-SN-025	LMC689.24.78N	5:07:07.33	-54:57:24.6	6721.58127	20.34	-	Ia	1.00	-	-	-	1.55	-	2.10	2.74	S	Ia
14-SN-026	LMC697.18.174N	5:22:13.47	-56:46:47.6	6721.55699	20.10	-	IIP	0.70	-	-	-	2.13	-	2.37	5.15	S	IIP
14-SN-027	MBR164.04.58N	2:41:49.91	-78:24:41.8	6728.51211	18.62	-	IIn	0.41	-	-	-	0.94	-	0.94	2.41	S	unknown
14-SN-028	LMC635.01.33N	5:09:42.76	-76:41:29.6	6734.55975	20.17	-	-	-	-	-	-	0.40	-	0.46	2.58	EII	-
14-NOVA-01	BLG643.22.8N	17:55:20.27	-23:23:54.5	6735.89972	16.29	-	-	-	-	-	-	-	-	-	-	-	-

Table 6: Properties of all transients found by the OGLE-IV Transients Detection System in seasons 2012-2014. See main text for details.

### 3. Classification of transients

During the real-time detection in years 2012-2014 the transients were classified only by a human observer and were split into two classes of candidates: supernovae or novae, typically relying on contextual information (primarily by checking if there was a galaxy-like object nearby) and the observed amplitudes. More robust and detailed classification can be performed either *via* spectroscopy while the transient is still on-going, or after the event is over and the full light evolution can be used for distinguishing transient classes. Below we describe those two channels.

#### 3.1. Spectroscopy

OGLE-IV transients appeared on the web-site after being found in the last-night's data (typically sooner than 12h after the last observation) and were immediately available for the astronomical community for the follow-up. Spectroscopic follow-up was carried out mostly by the Public ESO Survey PESSTO<sup>3</sup> (Valenti *et al.* 2012, Fraser *et al.* 2013, Smartt *et al.* 2013), using the New Technology Telescope (NTT) at La Silla Observatory, located about 20 km from Las Campanas. On a few occasions, however, OGLE transients were classified by PESSTO during the same night they were discovered, allowing for early confirmation of their nature and providing useful observational data for studying the early stages of supernova evolution. Another two sources of spectroscopic classification of the OGLE transients were the Carnegie Supernova Project (CSP, Hamuy *et al.* 2006) using the 6.5m Magellan Telescope and 100 inch Du Pont telescope in Las Campanas Observatory, and observers from the Australian National University (ANU) using the Wide-Field Spectrograph (WiFeS) at ANU 2.3m telescope in Siding Spring Observatory. The spectra of the OGLE supernovae classified by PESSTO are available *via* WiseRep repository (Yaron *et al.* 2013), whereas all the remaining spectra should be available from the respective groups. Spectral typing, redshifts and reference to the relevant classification telegram are given in Table 1.

Out of 238 transients reported by OGLE-IV real-time pipeline since 11th October 2012 until end of the 2013/2014 season (March 2014), 87 were classified spectroscopically and 83 turned out to be supernovae. Among those there were 47 Type Ia, 27 Type II (including 10 Type IIn and 2 Type IIp), as well as single examples of Ib, Ibn, Ic and peculiar Ia and Ic. The redshift range was from 0.014 (OGLE12-009) to 0.14 (OGLE13-043) for supernovae and up to 0.168 for AGNs (OGLE13-088). Table 1 contains information on the spectral classification and derived redshift. Examples of different types of supernovae and CVs are shown in Figs. 6 and 7.

---

<sup>3</sup><http://www.pessto.org>

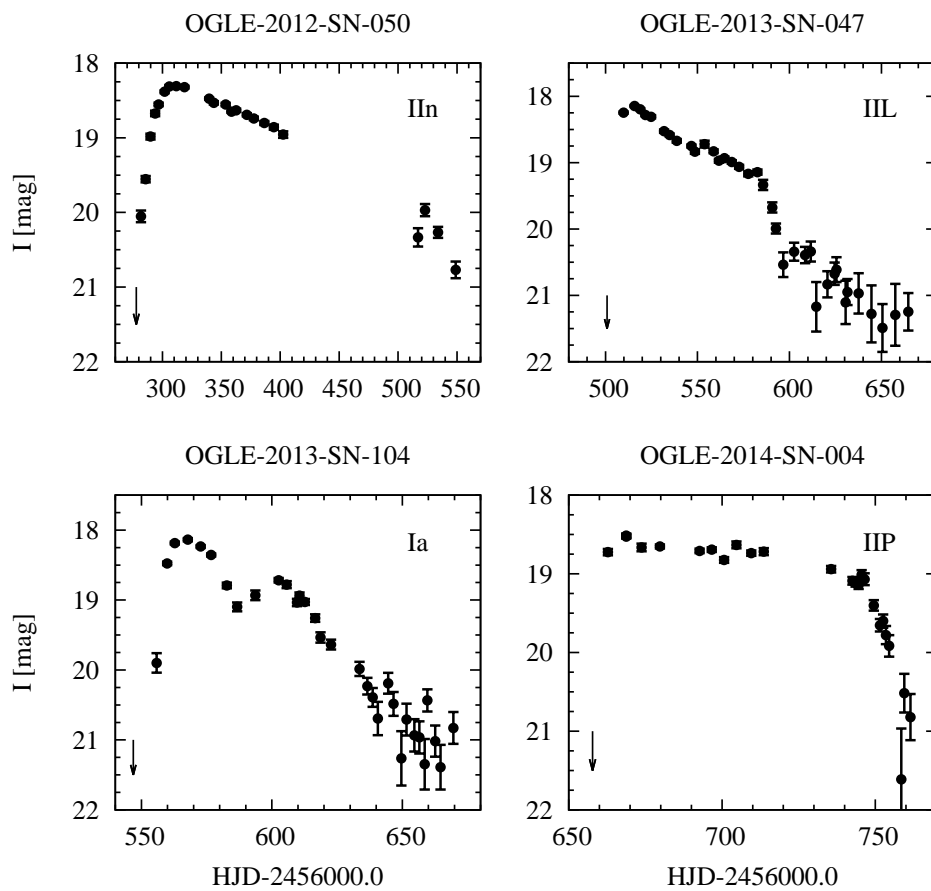


Figure 6: Examples of various spectroscopically determined supernova types among transients detected by the OGLE-IV Transients Detection System.

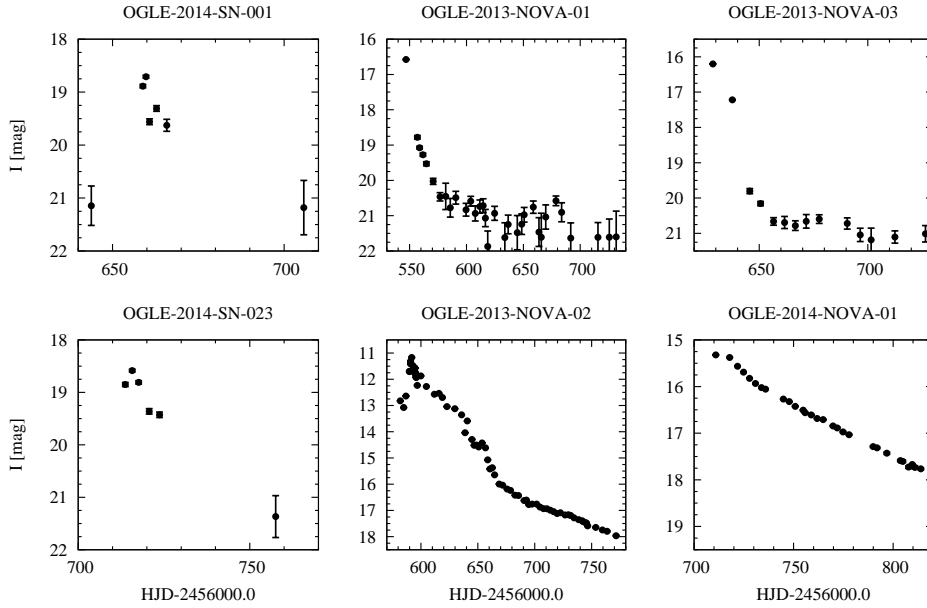


Figure 7: Examples of Novae and Dwarf Novae detected by the OGLE-IV Transients Detection System.

### 3.2. Photometry and Machine Learning Classification

Thanks to its relatively high cadence, OGLE-IV provides well sampled light curves of supernovae and other transients in the  $I$ -band and more sparse light curves in  $V$ -band. Therefore, the data can reveal characteristic features allowing us to distinguish between different supernova classes and cataclysmic variables. In particular, obtaining an early preliminary classification of a transient candidate could be helpful in allocating limited spectroscopic follow-up resources. Within the OGLE-IV Transients Detection System pipeline we typically detect transients near or just after their maxima, and there are at least a couple of data points available, as well as the time of the last non-detection. Here we present and test the performance of an automated light curve classifier, which uses such incomplete early data as input. This classifier will be implemented in the processing and detection chain in subsequent observing seasons.

In order to build a training set for the classifier we used both spectral classification and (somewhat subjective) visual classification of the full light curves and separated our findings into five major classes of transients: supernovae Type Ia (Ia), core-collapse supernovae of Type II $n$  and II $p$ , dwarf novae (DNe) and classical novae (CNe). The visual inspection was carried out by multiple experienced observers and relied on identifying crucial features of each of the classified types (*e.g.*, second maximum in SNe Type Ia), as well as contextual information (*e.g.*, presence of a

galaxy near the transient and galaxy type). The results of the visual classification are listed in Table 1 under *comment* column. The visual classification was attempted on the entire set of transients, however, still many objects remained classified as *unknown*. Among those visually classified, we selected about a dozen from each class to construct the training set. We would like to emphasize here the advantages of the OGLE data collected in the *I*-band, which allow to maintain high purity of the photometric classification thanks to clear second maximum present in SNe Type Ia and well sampled light curves.

Because there were only a couple of Dwarf Novae found by the Transient Detection System (usually discarded during the detection process and not reported on the web-site), for training we used a set of synthetic light curves, generated from a linear rise and exponential decline model of a DN outburst based on several dozens of DNe found in the OGLE-III data by Skowron *et al.* (2009). Several light curves were excluded from the training set because they had no pre-maximum data or the last non-detection date was unknown (for the very first transients). The training set for the automated classifier comprised of 63 objects of Type Ia and II SNe, CNe and about a hundred of simulated DNe, adjusted to the OGLE-IV sampling. Each light curve in the training set was trimmed at its maximum to mimic its typical appearance at the discovery epoch. For such data we computed the following set of features:

- slope1- slope in mag/d before the max,
- mag1- the maximum observed brightness,
- time2max- time to reach the maximum from the last non-detection,
- rise- difference in mag between the max and the detection level.

We classified the *I*-band photometry using a Random Forest classifier (Breiman *et al.* 2001) as implemented in the Weka package<sup>4</sup>. Random Forest (RF) takes as an input a set of values, which can represent any feature of the light curve. We trained the RF model on the training set and then classified all light curves with trained model. The highest ranked (winner) class and its probability are provided in Table 1 in the *phot.class* column, along with its probability (*prob.* column). Note, the light curve classification was performed in the observer frame, however, this had a negligible impact on the result as the redshifts of most of our extragalactic transients were ranging from  $z=0.05-0.15$ .

There are in total 238 transients in our table, however, if we exclude all transients with uncertain visual classification or with not enough data points before the maximum brightness, we are left with 196 objects. Further on, if we exclude objects classified outside of our five classes (*e.g.*, AGNs), we are left with 143 classifiable

---

<sup>4</sup><http://www.cs.waikato.ac.nz/ml/weka/> Weka, version 3.6.5, developed at the University of Waikato in New Zealand

transients. Among those, 120 (84%) were assigned a class in agreement with the spectral and visual classifications. This is a very promising result, especially given the fact, that in some cases there was just 1 data point between a non-detection and the maximum brightness. Overall, the performance of the classifier is good enough to provide not only distinction between CVs and SNe, but also between thermonuclear and core-collapse supernovae and their major subtypes. The sample of CNe used for training of the classifier should, however, be extended in future, with new detections, but also possibly with the OGLE-IV data from the Galactic bulge (Mróz *et al.* 2014) after resampling. Nonetheless, the classifier was able to make similar decisions to a skilled human, indicating its efficacy. Future improvements could include adding new features, such as the presence of a host and WISE colors.

The Random Forest classifier performed relatively well on known five classes. For the other classes of transients, *e.g.*, OGLE-2012-SN-006 classified spectroscopically as Ibn (Pastorello *et al.* in prep.), or OGLE-2013-SN-066 which was likely an AGN flare, the classifier returned the winning class from the five trained classes, however, usually the broad probability distribution function (PDF) indicated the uncertainty of the classification. The highest value in the PDF and corresponding class are shown in Table 1 for those objects.

In the future, in order to increase the capabilities of the classifier, the training set should be expanded with more examples of cataclysmic variable outbursts and also a wider variety of Type II supernovae. Nevertheless, we have shown that applying a very simple feature-based classification, we were able to reasonably well reproduce the classification from spectra or full light curve inspection. This classification schema will be implemented within the OGLE-IV pipeline in future observing seasons.

#### 4. Supernovae Environments

The majority of the SNe from the OGLE sample are located within or close to galaxies. The host-galaxy properties and the supernova environment is a plausible source of inhomogeneity in SN properties (*e.g.*, Maguire *et al.* 2011; Childress *et al.* 2013), with a probable dependence on redshift since the galaxies evolve with redshift.

In order to compute the projected distances of our supernovae from the centers of their host galaxies, we first modeled the hosts' light profiles with an elliptical Sérsic profile with Sérsic index  $n$  free to vary using the *galfit* software (Peng *et al.* 2002). Models were obtained for hosts of 148 transients (the rest had either not present or too faint hosts) and we measured the position of the nucleus as well as an effective radius encompassing half of the total galaxy flux, denoted  $R_{\text{Ser}}$ . In Fig. 8 we present examples of fitted galaxies (OGLE-IV reference image, the best fit model, and the residuals). The positions of supernovae were derived using the subtracted images from the DIA pipeline (which, by definition of the difference

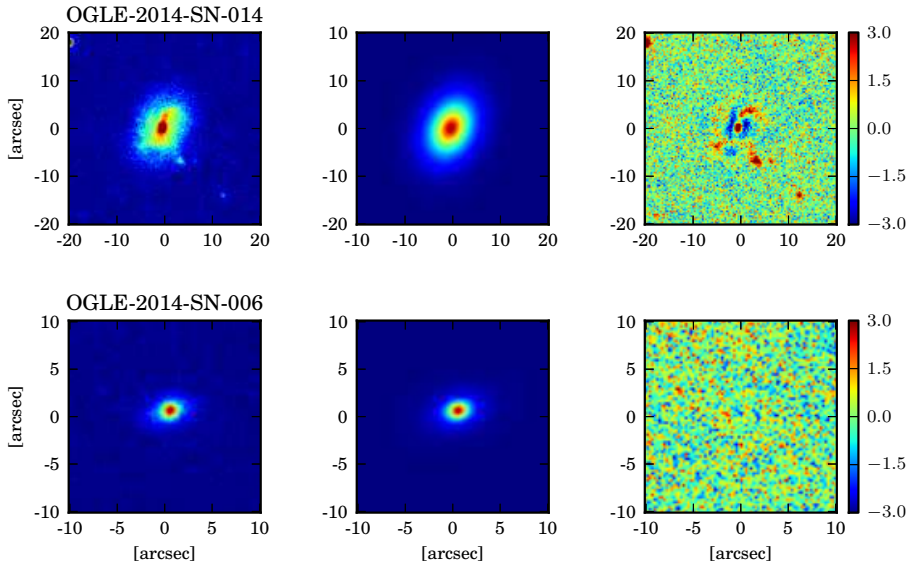


Figure 8: Examples of *galfit* models of the light of the host galaxies. The leftmost panel shows the original images from the OGLE-IV reference images, the middle are the models and the residuals are on the right. The scale of the residuals is normalized to one sigma. The upper example shows a galaxy with spiral arms, not well modeled by *galfit*, whereas the lower example is a galaxy well approximated by a single component ellipsoidal model.

imaging, were registered on the same grid as the reference images), with the residuals fitted with the Gaussian profile. The angular offset between the supernova and its host's nucleus is listed in Table 1, as well as the projected separation in kpc for cases with known distance (*via* redshift). Fig. 11 shows the distribution of angular distances for 148 transients with successful *galfit* models in arc seconds. We also added a distribution of 110 transients classified as very likely supernovae in the visual and spectroscopic classification. The distance distribution clearly shows that OGLE-IV Transient Detection System program is finding most of its transients near or on top of the cores of the galaxies. This is achieved thanks to superb image quality of the OGLE survey and a dedicated difference imaging software fine-tuned to the survey's data.

Galaxies vary in morphology and size, hence in order to obtain a more homogenous picture of the distribution of supernova separations we normalized the distance between a SN and its host using the Sérsic radius, taking into account the ellipticity and orientation of the galaxy. Table 1 contains the Offset\*, which is computed across isophotes of the galaxy light profile, such that, *e.g.*, for an edge-on galaxy, a supernova located below or above the most of the light of the galaxy

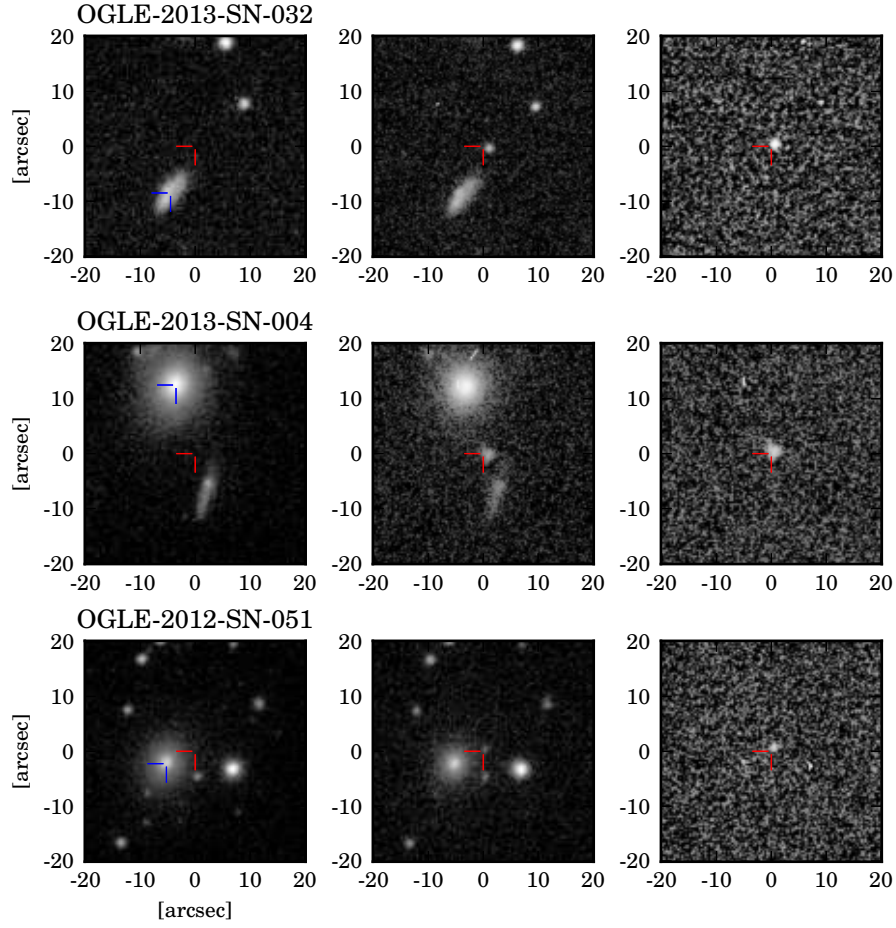


Figure 9: Examples of spectroscopically confirmed supernovae separated by more than  $3R_{\text{SER}}^*$  from the host center. From left to right: reference image, maximum brightness image, subtraction image. The red cross marks the centroid position on the subtracted image and the blue cross is the center of the galaxy from the *galfit* model.

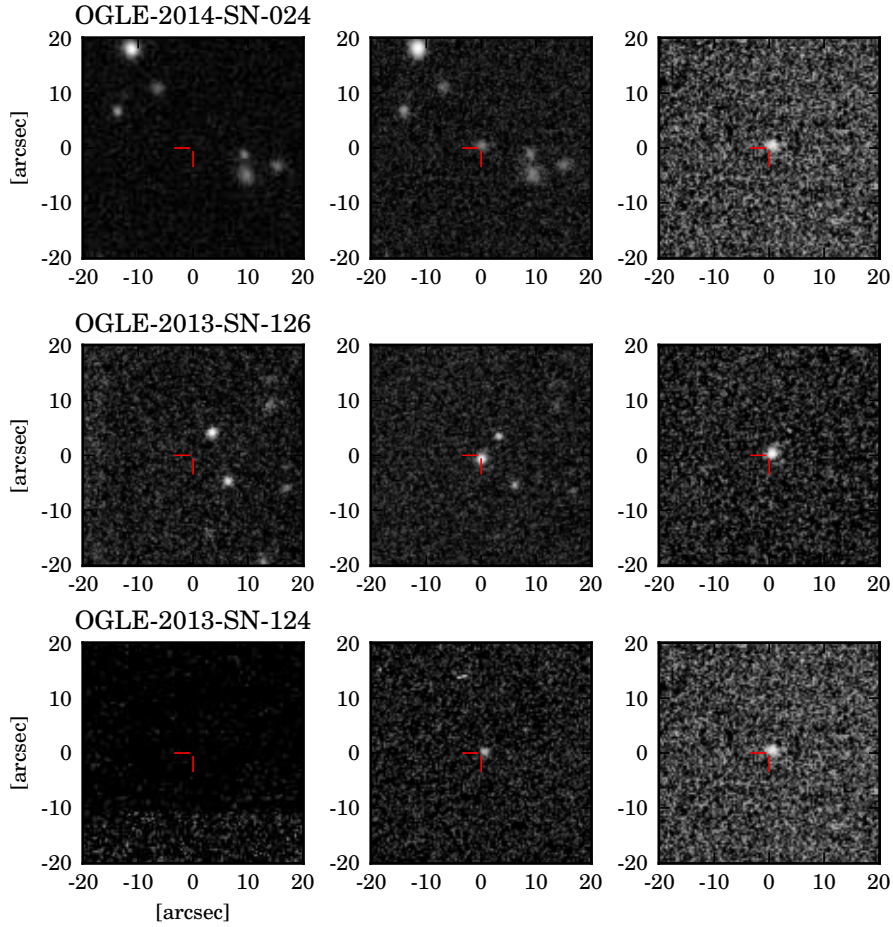


Figure 10: Examples of apparently host-less supernovae with spectral confirmation as Type Ia. From the left to right: reference image, maximum brightness image, subtraction image. Red crosses mark the position of the centroid of the subtracted object.

will have its Offset\* larger than another supernova at the same angular distance, but located along the galaxy disk. Fig. 12 shows examples of spectroscopically confirmed supernovae which were detected at a galactocentric distance larger than 3 Sérsic radii computed across isophotes ( $R_{\text{SER}}^*$ ). Fig. 10 shows supernovae classified as Type Ia for which the host was not found within 30 arc seconds from the transient. In most cases the host was probably too faint and was not detected on OGLE reference images (depth  $\sim 22$  mag, which corresponds to  $M_I < -16$  mag), however in some cases the host could have been located at a much larger separation (*e.g.*, OGLE-2013-SN-006).

In the Fig. 11 we present the distribution of separations between the transient

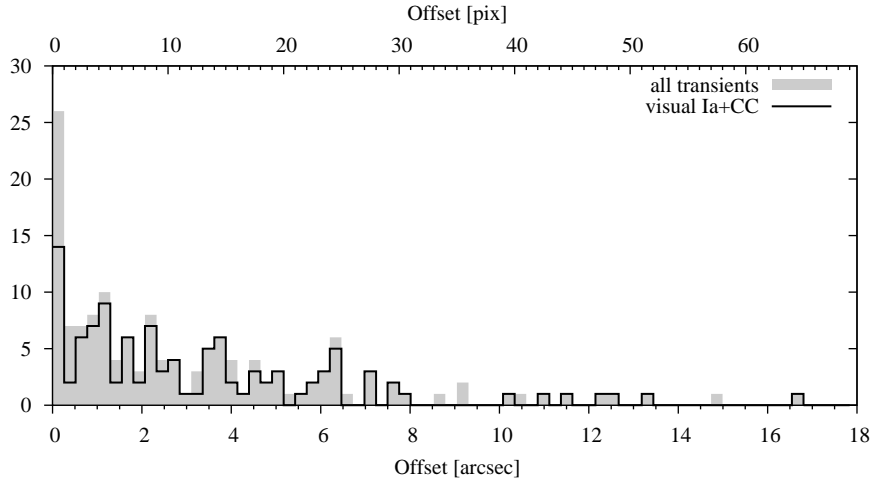


Figure 11: Distribution of distance between the transient and the galaxy centre of light in arcsec and OGLE-IV pixels (0.26 arcsec) - gray: all 148 models and black line: 110 visual confirmed SNe. About half of the transients from 26 found within radius of 1 pixel (0.26 arcsec) from galaxy center are most likely AGNs (based on spectra, previous variability or WISE colors), but we still find a significant number of SNe in the galaxy centers.

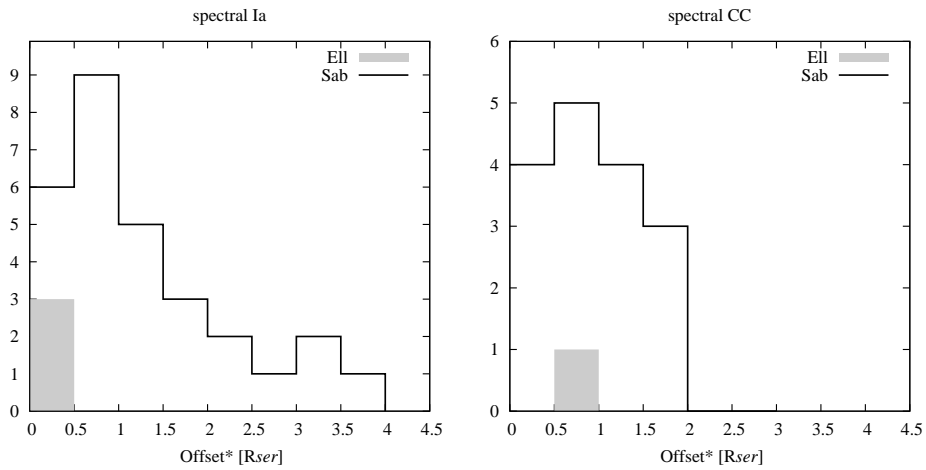


Figure 12: Distribution of distance between the transient and the galaxy centre of light normalized with Sérsic radius for: visually and spectroscopically confirmed Type Ia and CC SNe. The transients are also divided by the host galaxy type - spiral or elliptical - based on WISE colors classification.

and the galaxy centre in arc seconds for two samples: all transient candidates with visible hosts and transients visually and spectroscopically classified as supernovae. After removing AGN candidates, we can see that there is still a number of transients being found in the very centers of the galaxies, what we discuss below.

In Fig. 12 we show the galactocentric separations of supernovae in units of the Sérsic radius only for spectroscopically confirmed supernovae. We distinguish between Type Ia and CC supernovae and separate the hosts between spiral and elliptical galaxies, based on WISE colors, following the method of Assef *et al.* (2010) and Kozłowski *et al.* (2013). We notice that the majority of OGLE SNe are found in spiral galaxies. The distribution follows the light in galaxy and half of the events lies within a single Sérsic radius. Deficit of supernovae below 0.5 half-light radii is mostly caused by a selection bias of the spectroscopic follow-up observations, which tend to avoid nuclear transients.

#### 4.1. Galaxy Orientation Bias

Inclination plays an important role in SN detection. Spiral galaxies with higher inclination have higher surface brightness and higher extinction along the line of sight. Therefore, we should expect an observational bias toward finding more supernovae toward less inclined galaxies. We have used the galaxy short-to-long axis ratio  $q = b/a$  obtained from *gal fit* to compute the galaxy inclination for the sample of OGLE spiral galaxies. The usual Hubble (1926) formula has been used, adopting the median short-to-long axis ratio  $\gamma = 0.22$  derived by Unterborn and Ryden (2008) and the correction of  $+3^\circ$  from Aaronson *et al.* (1980).

$$i = \cos^{-1} \left[ \sqrt{\left( \frac{q^2 - \gamma^2}{1 - \gamma^2} \right)} \right] + 3^\circ \quad (1)$$

The resulting normalized distribution of OGLE SN hosts inclinations is shown in Fig. 13, along with the normalized distribution of a random selection from the overall galaxy population. We observe a gap in the low inclination regime (*i.e.*, face-on galaxies). This effect has already been observed in other surveys (Leaman *et al.* 2011) and it is associated with lack of precision when measuring the major and minor axis. In the case of randomly oriented galaxy sample, we should expect a uniform distribution in  $\sin(i)$ ; however, the precision issue makes this assumption no longer valid.

To analyze the distribution of inclination angles for the SN host population, removing any possible systematic bias associated with the uncertainty in the inclination angle, we compared two populations: the first containing SN host galaxies and the second containing a random sample of galaxies (*i.e.*, contained in the OGLE field LMC571, as published in Soszyński *et al.* 2012), which have also been modeled with *gal fit*. In order to account for spiral galaxies only, we selected only the galaxies with Sérsic index  $n < 2$  from both groups. The cumulative distribution of  $\sin(i)$  for both populations is plotted in the right panel of Fig. 13. The figure,

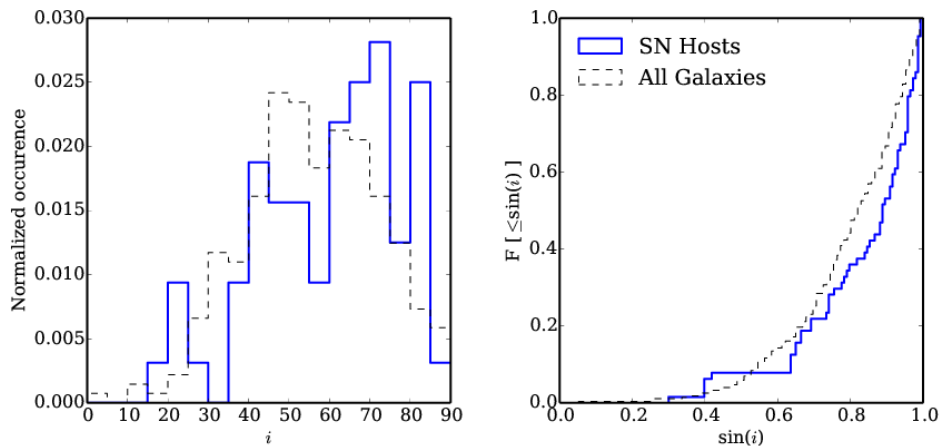


Figure 13: Left: Histogram of computed inclinations for a SN host galaxy population (blue thick line), and histogram for a random sample of spiral galaxies (thin black line). Right: Cumulative normalized distribution of  $\sin(i)$  for both populations.

contrary to our expectations, shows an excess of objects with higher inclinations (approximately higher than  $45^\circ$ ) among the SN hosts, meaning that the edge-on orientation are more frequent among SN hosts. In order to quantify this effect, we run a Komolgorov-Smirnov two population test, which provides a  $p$ -value=0.1078. This result means that with a significance of 10% we can not rule out the null hypothesis that the two populations are identical. The conclusion is that there is no a statistically significant host galaxy bias in our sample.

#### 4.2. Positional Accuracy

The main source of uncertainty in the galacto-centric distance measurement comes from the galaxy light modeling. Positions of transients are derived from the DIA subtracted images and are typically known to better than a fraction of a pixel. In order to assess uncertainty of the nucleus position we used a sample of AGNs, which are located at the centers of galaxies. We selected the AGNs based on their mid-IR colors as measured by WISE (Assef *et al.* 2010) and picked those which also exhibited a clear variation in their light curves. For the ten brightest data points we extracted the mean position of the DIA residuals. Then, it was compared to the position of the center of the host galaxy derived using *galfit*. We only considered nearby AGNs ( $z < 0.15$ ) where the host galaxy was clearly visible on the OGLE reference images. For the selected sample of 16 AGNs (see Fig. 14) the measured offsets in the  $x$  and  $y$  coordinates were smaller than 0.5 pixel (0.13 arc sec). As this verification method also included the uncertainty in the transient position as measured in difference images (DIA), we find that the overall error budget for our

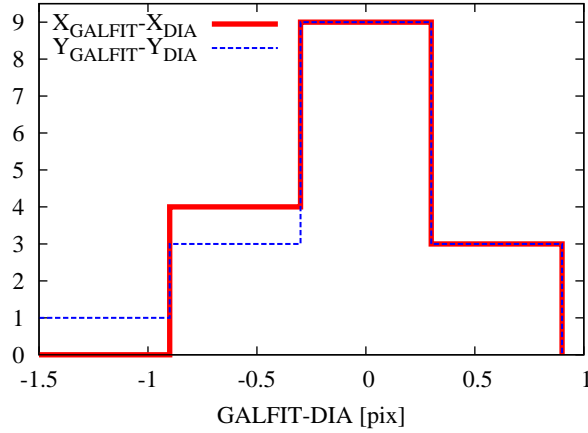


Figure 14: Difference in  $x$  and  $y$  coordinate between *galfit*-measured center of a galaxy hosting a central AGN and a DIA-based position of the residuals at the maximum brightness of the AGN. The sample comprises of 16 AGNs, for which the  $\langle \Delta x \rangle = -0.071 \pm 0.355$  pixels,  $\langle \Delta y \rangle = -0.073 \pm 0.379$  pixels. 1 pixel is 0.26 arc seconds.

distance determination using *galfit* and the DIA is about 0.13 arc seconds for a typical transient of 18-19 mag.

#### 4.3. Transients in the Centers of Galaxies

Interestingly, there seem to be at least a dozen of transients found within the centers of their hosts (within 1 pixel of the center) which were not classified as supernovae, neither spectroscopically nor visually. Partially, the reason for the deficit of spectroscopically observed transients near the centers of galaxy is the natural bias of the follow-up groups, which tend to avoid taking spectra near the centers of galaxies due to centering and contamination with host galaxy light. Nevertheless, the excess of central transients in Fig. 11 is clearly visible. Those are probably for the most part flares or other photometric activity of AGNs, with the most obvious examples being OGLE13-088 and OGLE13-090, for which their AGN nature was also confirmed with spectroscopy. We also used WISE color cuts to classify transients as potential AGNs following the method of Assef *et al.* (2010), shown in Table 1 under WISE column. Some of the central transients, however, do not seem to correspond to an AGN identified within the nucleus of the host, *e.g.*, OGLE13-066 or OGLE13-033. Among those transients located within one pixel from the nucleus is one (OGLE13-071) with a light curve resembling that of a Tidal Disruption Event (TDE, *e.g.*, Gezari *et al.* 2012), but somewhat shorter with duration of only about 70 days. More interestingly, there are also two other short events which appeared in the centers of galaxies: OGLE13-003 and OGLE13-056, which lasted for less than 40 days, see Fig. 15 for their light curves. It is currently difficult to

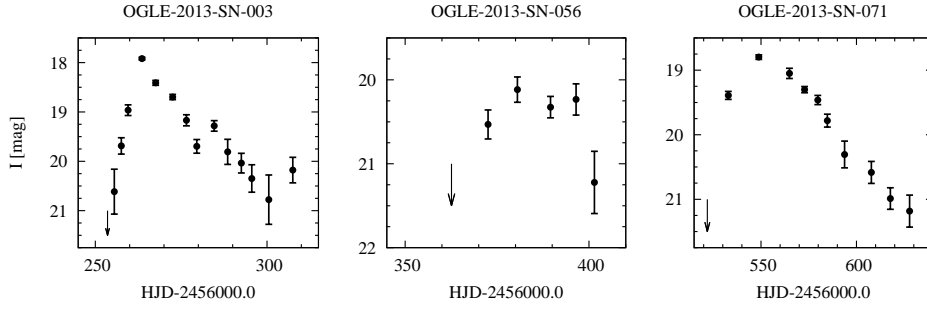


Figure 15: Nuclear transients of not obvious nature found within 1 pixel (0.26 arcsec) from the cores of their hosts.

conclude upon their nature with no spectroscopic follow-up, however, we can expect similar transients being found in the OGLE data in the following seasons, and hope for real-time detections of TDEs and other exotic nuclear transients, allowing their detailed studies.

#### 4.4. *Supernova Factories*

We note that among all OGLE transients, there were two pairs of supernovae which exploded in the same host galaxy. Such cases are important for studying supernovae environments and the supernova rates (*e.g.*, Thöne *et al.* 2009). The first pair, OGLE-2013-SN-017 and OGLE-2014-SN-014, appeared clearly in the

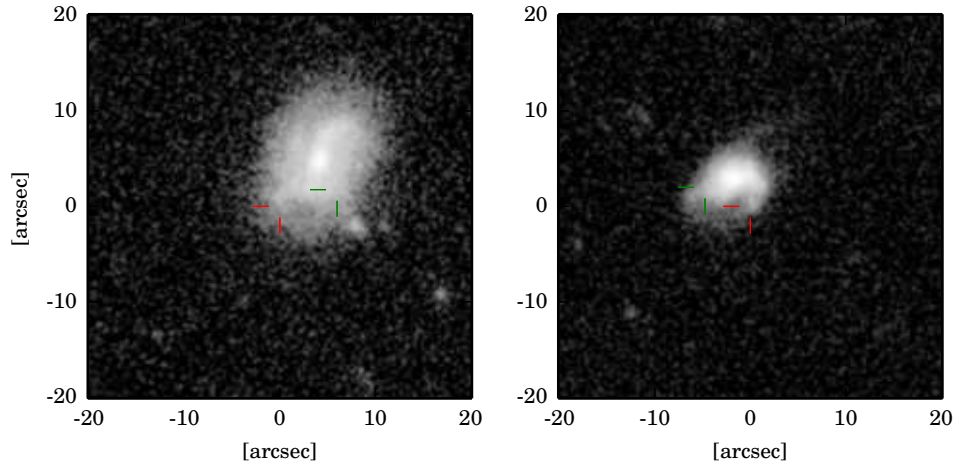


Figure 16: Supernova factories: galaxies with two supernovae found within one and two years, respectively. Left: Type II<sub>n</sub> OGLE-2013-SN-017 (green) and type Ib OGLE-2014-SN-014 (red). Right: OGLE-2011-SN-034 (green) (from Kozłowski *et al.* 2013) and OGLE-2013-SN-022 (red), both of unknown types.

same host, the galaxy 2MASX J04272268-7442059 (after NED), separated by 6.36 arcseconds, *i.e.*, 5.3 kpc at  $z=0.043$ . SN OGLE13-017 was classified as a Type II<sub>n</sub> (Inserra *et al.* 2013), and the other one, which exploded about a year later, SN OGLE14-014 was also core-collapse, type Ib (Marion *et al.* 2014). The second pair, OGLE-2011-SN-034 and OGLE-2013-SN-022, consists of an archival (Kozłowski *et al.* 2013) and real-time detections. The separation in this case was 5.22 arcsec, however, neither of those supernovae were classified, nor we know the redshift of the host galaxy (GALEXASC J025017.60-705225.4 after NED). Their light curves are not completely covered, therefore their photometric classification is also difficult, however, most likely they both are SNe Type Ia. The reference images with hosts and positions of paired supernovae are shown in Fig. 16. We note, that there is also an apparent pair: OGLE-2013-SN-034 and OGLE-2013-SN-055, which are the same supernova, but given two separate IDs by mistake.

### 5. Cosmology with OGLE Supernovae

A key goal of most supernova surveys is detecting Type Ia supernovae, which are known to be “standardizable candles”, and hence can be used for cosmological studies of the expansion of the Universe (*e.g.*, Riess *et al.* 1998, Perlmutter *et al.* 1999, Sullivan *et al.* 2011, Campbell *et al.* 2013). Our sample from the OGLE-IV survey consists of 49 spectroscopically confirmed Type Ia SNe within the redshift  $z < 0.14$  with a median value of  $z=0.076$ .

The absolute magnitude of the SN observed at magnitude  $m$  is described by the equation:

$$M = m - \mu - A_{MW} - A_H - K(z), \quad (2)$$

where  $\mu$  is the distance modulus,  $A_{MW}$  and  $A_H$  are the extinctions in the Milky Way and in the SN host galaxy in the  $I$ -band, respectively. The single filter  $K$ -correction, which accounts for brightness difference due to redshifted spectrum, was adopted from the Magellanic Bridge supernova sample in the OGLE-IV (Kozłowski *et al.* 2013). The distance moduli to the SNe were calculated from spectroscopic redshifts assuming the  $\Lambda$ CDM cosmological model from the Planck mission with parameters:  $H_0 = 68$  km/s/Mpc,  $\Omega_M = 0.31$ ,  $\Omega_\Lambda = 0.69$  (Planck collaboration 2013). We took into account the Milky Way extinction toward each SN using Galactic Extinction maps from Schlafly and Finkebeiner (2011) (retrieved *via* the NASA/IPAC Extragalactic Database). Due to lack of color light curves we were not able to fit the color for our light curves, hence the host galaxy extinction remained as the only unknown parameter.

The distance moduli were also derived from the light curve fitting and here we used the empirical method for fitting multi-color light curves of Type Ia SNe described by Prieto *et al.* (2006). This method relies on the calibrated relation between the absolute magnitudes at maximum light and the post maximum decline rate  $\Delta m_{15}$  (brightness change from maximum to 15 days post maximum) in  $BVRI$

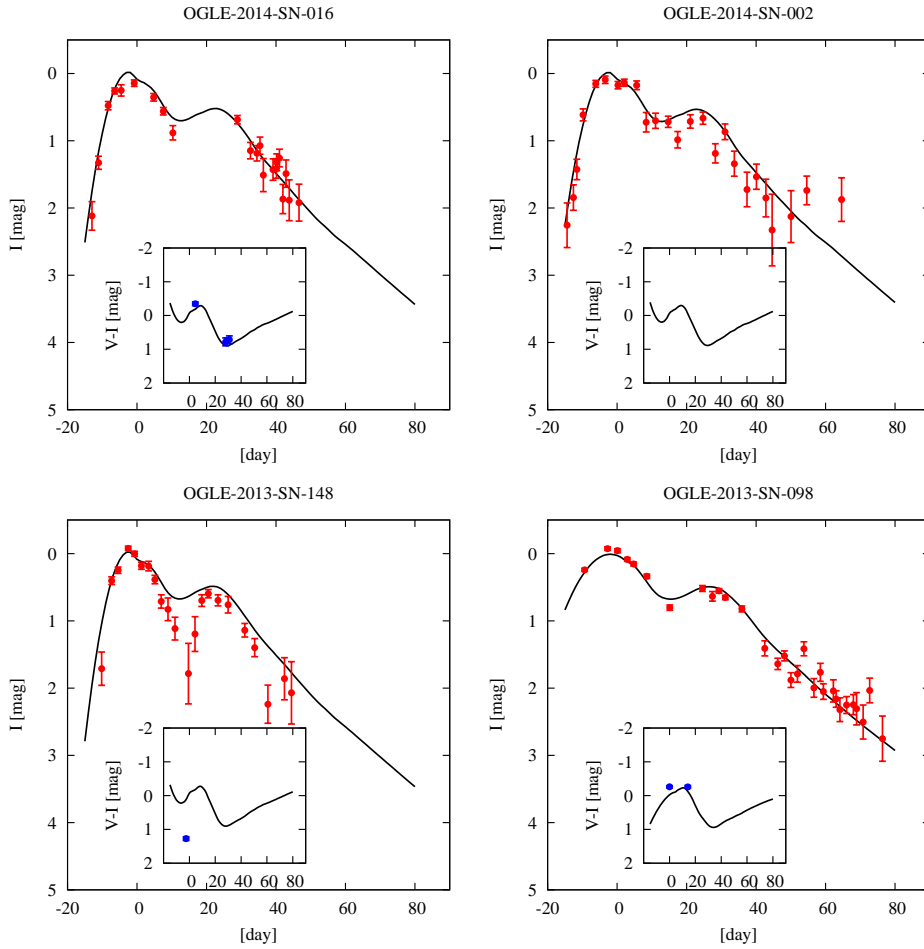


Figure 17: Example light curves of Type Ia supernovae from OGLE-IV along with their models from Prieto *et al.* (2006) (black solid line). The time axis shows days from the  $I$ -band maximum. The inset in each panel shows the available  $V - I$  data with the model. Supernova OGLE-2013-SN-148 exhibits a very deep dip between the two peaks and its model is poorly fitted. Also its color around maximum is significantly redder than other supernovae, indicating a significant amount of extinction.

filters. By fitting the parameter  $\Delta m_{15}$  and using the linear relation between the absolute magnitude at maximum and the post maximum decline rate we obtained the absolute magnitude, and hence the distance moduli for our supernovae. For fitting we used the well sampled  $I$ -band light curves and, where available,  $V$ -band data. In Fig. 17 we show examples of OGLE Type Ia supernovae and the best fitted template from Prieto *et al.* (2006).

In Fig. 18 we present the Hubble Diagram for 49 Type Ia SNe from the OGLE

sample with spectroscopic redshifts. The final error in the distance modulus is obtained by adding in quadrature the instrumental error in measured magnitude, the scatter of fitting SNe templates, and the dispersion in  $\Delta m_{15}$  (Prieto *et al.* 2006). We compared our data to the  $\Lambda$ CDM cosmology model with Planck parameters (Planck collaboration, 2013) and obtained the scatter of 0.315 mag in residuals. Table 7 presents the results of the  $\Delta m_{15}$  fits to the light curves of 49 Type Ia SNe in the OGLE sample with the columns with  $\Delta m_{15}$  value, the distance modulus derived from  $\Delta m_{15}$ , residuals on the Hubble diagram for the Planck cosmological models, the isophotal offset between a SN and the galaxy center (where the light model was available) in units of the Sérsic radius.

The Hubble Diagram residuals exhibit relatively low scatter of 0.315 mag, despite the fact that the results relied on single-band light curves. However, our light curves were in most cases well covered from before the maximum until the supernova disappeared, allowing for good template fitting. The residuals exhibit clearly a systematic positive offset, which is expected, as we did not include any host galaxy extinction in the distance moduli calculations. Ignoring other more subtle effects on the residuals, like the host mass or metallicity, we can therefore use them to infer the amount of the host extinction for each of the supernovae. The most striking outlier is supernova OGLE13-148, which exhibits the most significant deviation from the expected brightness by more than 1 mag. Also, a single  $V - I$  measurement near the first peak indicates the host extinction was very large in this case, but the finding chart shows that this supernova appeared on top of a well-pronounced spiral arm of a large galaxy. On the other hand, as seen in Fig. 17, the model of the light curve of OGLE13-148 matches well everywhere except for the dip between the two  $I$ -band peaks. However, the significant dip by more than 1 mag is hard to explain even by somewhat higher extinction, and this object requires more detailed studies.

In Fig. 19 we show the offsets between supernovae locations and their host galaxy centers against their residuals on the Hubble Diagram. We notice a subtle increase in the residuals while approaching the normalized center of the host galaxy, however, after about two half-light radii the residuals tend to agree with zero. Ignoring the larger scatter in the residuals below  $0.1 R_{Ser}$  and a few negative residuals, likely due to inaccuracies in galaxy core subtraction, we can see that in range from  $0.1$  to  $2 R_{Ser}$  the systematic offset can be approximated as constant. Assuming it is all caused by the host extinction we can derive a mean value of the extinction for this range of normalized galactocentric separations of  $A_I = 0.19 \pm 0.10$  mag. Based on the relation between  $A_I$  and  $A_V$  from Rieke and Lebofsky (1985) we derive  $A_V = 0.39 \pm 0.21$  mag, in agreement with Galbany *et al.* (2012) who obtained the mean value of  $A_V = 0.36 \pm 0.02$  mag for the SDSS sample of Type Ia SNe in spiral galaxies. They have also derived a linear dependence of extinction on the projected distance from the host galaxy center, however, we do not see this trend in our data.

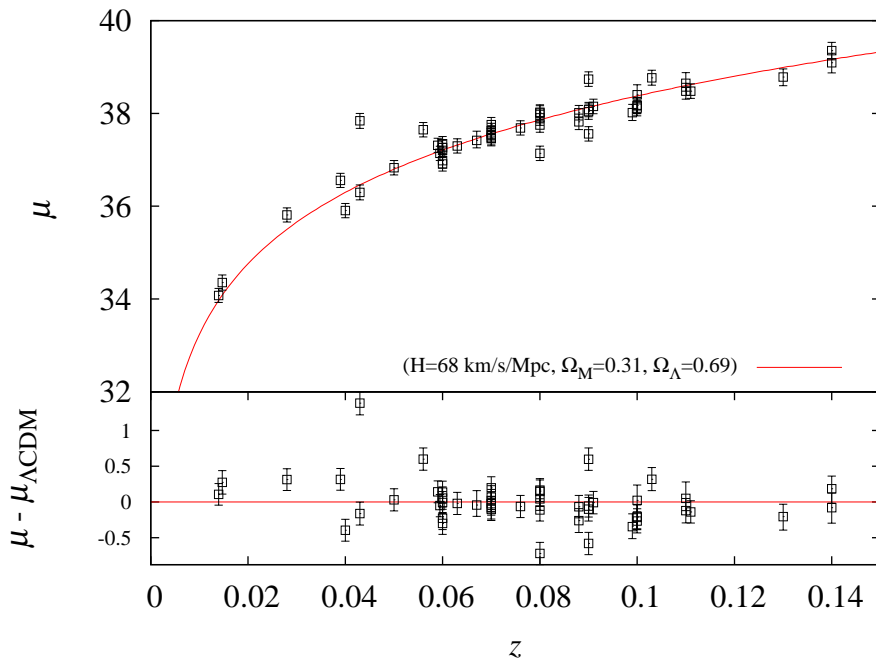


Figure 18: Top: Hubble diagram for the OGLE sample: the distance modulus–redshift relation ( $\mu_{\Lambda\text{CDM}}$ ) of the assumed  $\Lambda\text{CDM}$  cosmological model from Planck. Bottom: Residuals from the assumed  $\Lambda\text{CDM}$  cosmological model as a function of redshift. Mean offset and its *rms* is  $0.004 \pm 0.315$ .

For OGLE-IV Type Ia supernovae located between 0.1 and 2 half-light radii from the host centers we used the derived correction for the extinction and for the rest we assumed no or negligible extinction. Hubble Diagram with the Union 2.1 sample of supernovae (Suzuki *et al.* 2012) and 49 supernovae from OGLE-IV is shown in Fig. 20. Except for a couple of clear outliers due to very high extinction or bad models, our ensemble of supernovae fits well within the “gold-sample” of cosmologically useful supernovae Type Ia, complementing the sample in the least populated redshift range from 0.06 to 0.11.

## 6. Summary

Since 2010, the OGLE-IV survey has been annually discovering  $\sim 150$  transients in the regions of the sky around the Magellanic Clouds. The OGLE-IV Transient Detection System surveys  $650 \text{ deg}^2$  of the sky to a depth of  $I < 21 \text{ mag}$  from 2012 and provides an unbiased sample of all types of supernovae to  $z \sim 0.15$ . Excellent data quality provided by the state-of-the-art fine-tuned difference imaging delivers high quality and well sampled light curves, as well as discoveries from a range of galactic environments, including both very dense central and remote loca-

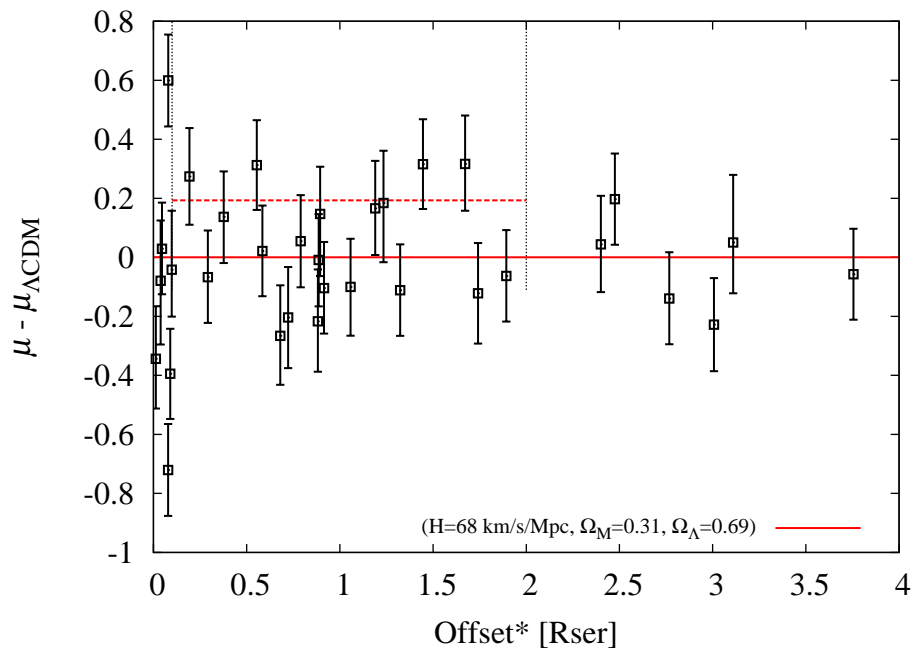


Figure 19: Residuals on the Hubble Diagram as a function of the offset between the SN location and the host galaxy nucleus in units of Sérsic radius. We show the results for 33 Type Ia SNe for which the hosts were detected and successfully modeled with *galfit*. The host extinction in the range between 0.1 and 2 half-light radii computed from the mean residuals is  $A_I = 0.19 \pm 0.10$  mag (dashed line) assuming Planck cosmological parameters. Central transients (distance below 0.1) exhibit significant scatter in residuals most likely due to inaccuracies in galaxy core subtraction.

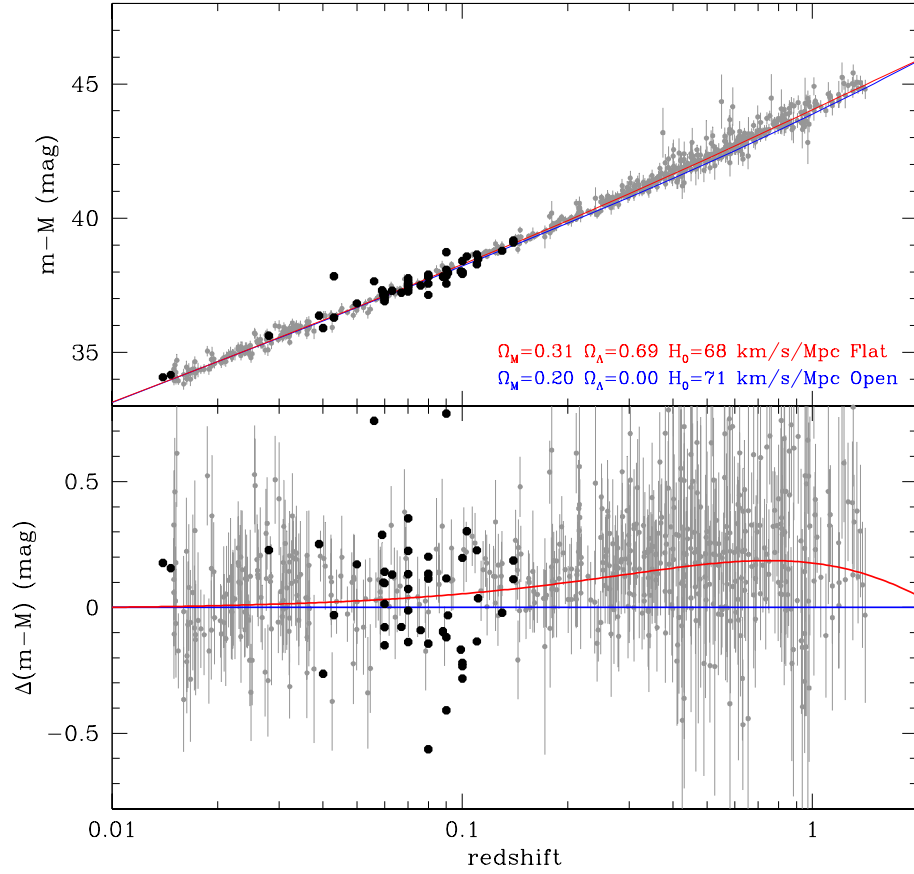


Figure 20: Hubble Diagram with OGLE-IV (black dots) and Union 2.1 sample (gray) of supernovae Type Ia along with Planck (flat) and open cosmological model. OGLE-IV supernovae were corrected for extinction based on their distance from the host center.

ID	$z$	$A_{MW}$	$\Delta m_{15}$	$\mu$	$\mu - \mu_{\Lambda CDM}$	Offset*
OGLE-20..		[mag]		[mag]	[mag]	[ $R_{Ser}$ ]
14-SN-024	0.1	0.244	0.839	38.403	0.028	
14-SN-021	0.039	0.113	1.183	36.556	0.321	1.45
14-SN-019	0.04	0.113	1.260	35.905	-0.39	0.09
14-SN-016	0.07	0.287	1.299	37.536	-0.019	
14-SN-010	0.056	0.109	1.247	37.649	0.604	0.08
14-SN-002	0.10	0.063	1.289	38.114	-0.261	0.68
13-SN-156	0.14	0.055	1.234	39.090	-0.074	0.04
13-SN-148	0.043	0.150	1.368	37.841	1.386	
13-SN-147	0.099	0.113	1.281	38.016	-0.339	0.01
13-SN-141	0.05	0.189	1.307	36.829	0.034	0.05
13-SN-136	0.080	0.065	0.860	38.026	0.171	1.19
13-SN-130	0.09	0.095	1.052	38.738	0.603	
13-SN-129	0.08	0.028	1.337	37.904	0.049	2.40
13-SN-126	0.06	0.051	1.246	37.202	-0.003	
13-SN-124	0.13	0.065	1.191	38.785	-0.2	
13-SN-123	0.08	0.078	1.457	37.139	-0.716	0.08
13-SN-120	0.07	0.113	1.644	37.628	0.073	
13-SN-118	0.07	0.113	0.882	37.757	0.202	2.48
13-SN-109	0.088	0.036	1.096	38.013	-0.062	0.29
13-SN-099	0.028	0.478	0.953	35.812	0.317	0.55
13-SN-098	0.06	0.044	1.068	37.347	0.142	0.38
13-SN-096	0.11	0.087	1.158	38.478	-0.117	1.74
13-SN-080	0.103	0.076	1.096	38.766	0.321	1.67
13-SN-075	0.08	0.038	1.117	37.748	-0.107	1.32
13-SN-073	0.091	0.057	1.257	38.151	-0.004	0.89
13-SN-070	0.043	0.029	1.734	36.297	-0.158	
13-SN-057	0.10	0.032	1.265	38.163	-0.212	0.88
13-SN-051	0.07	0.024	1.107	37.456	-0.099	0.92
13-SN-044	0.07	0.077	1.069	37.581	0.026	0.58
13-SN-043	0.14	0.031	1.025	39.354	0.189	1.23
13-SN-041	0.10	0.034	1.192	38.176	-0.199	0.72
13-SN-040	0.09	0.033	1.219	38.039	-0.095	1.06
13-SN-039	0.08	0.056	1.132	38.007	0.152	0.89
13-SN-032	0.09	0.035	1.097	38.083	-0.052	3.76
13-SN-018	0.067	0.113	1.441	37.418	-0.037	0.10
13-SN-015	0.088	0.051	1.714	37.819	-0.257	
13-SN-009	0.060	0.060	1.243	37.265	0.06	0.79
13-SN-004	0.06	0.140	1.415	36.982	-0.223	3.01
13-SN-001	0.09	0.026	1.266	37.559	-0.576	3.11
12-SN-051	0.11	0.045	1.482	38.650	0.055	
12-SN-049	0.07	0.056	1.303	37.477	-0.078	2.77
12-SN-046	0.111	0.050	1.182	38.480	-0.135	
12-SN-044	0.06	0.034	1.182	36.910	-0.295	
12-SN-040	0.014690	0.113	1.889	34.354	0.279	0.19
12-SN-032	0.063	0.113	1.216	37.299	-0.016	
12-SN-014	0.059	0.113	1.069	37.312	0.147	
12-SN-009	0.013966	0.046	1.063	34.076	0.111	
12-SN-007	0.059438	0.103	1.293	37.139	-0.046	
12-SN-005	0.076	0.042	1.207	37.687	-0.058	1.89

Table 7: Parameters of the 49 Type Ia supernovae modeled using Prieto *et al.* (2006) templates.  $A_{MW}$  is the Milky Way extinction in the  $I$ -band.  $\Delta m_{15}$  is the parameter obtained from the template fits,  $\mu$  is the derived distance modulus,  $\mu - \mu_{\Lambda CDM}$  are the HD residuals for different cosmologies and Offset\* is the galacto-centric distance of a supernova in units of the Sersic radius (only for hosts with good *gal fit* models).

tions.

We presented the data for all 238 transients found in real-time in years 2012-2014, among which a significant fraction were classified spectroscopically. Supernovae Type Ia were used to construct the Hubble Diagram with relatively small intrinsic scatter. Systematics in the residuals were also used to derive the mean value of host extinction in the range up to two half-light radii.

Projected galactocentric distances of most of the transients were measured, and we showed that OGLE-IV is capable of detecting nuclear transients with good efficiency. We presented a few examples of interesting central transients of unknown nature.

The OGLE-IV Transient Detection System is expected to continue in the future, extending the sample of well covered supernovae light curves and providing more interesting cases for detailed studies.

**Acknowledgements.** We thank Drs M. Fraser, D. Poznanski, H. Campbell for their continued support and help in preparation of this manuscript. We would like to express our gratitude to the members of the spectroscopic follow-up groups, especially the PESSTO team, CSP (in particular to E. Y. Hsiao, G. H. Marion and M. Phillips) and M. Childress (ANU).

We also would like to thank the fellows of the Polish Children's Fund, Jakub Aniolis, Jakub Banaszak and Jakub Mnich, for their involvement in this work.

This work made use of observations collected at the European Organisation for Astronomical Research in the Southern Hemisphere, Chile as part of PESSTO, (the Public ESO Spectroscopic Survey for Transient Objects Survey) ESO program ID 188.D-3003.

This research has made use of the NASA/IPAC Extragalactic Database (NED) which is operated by the Jet Propulsion Laboratory, California Institute of Technology, under contract with the National Aeronautics and Space Administration.

This publication makes use of data products from the Wide-field Infrared Survey Explorer (WISE), which is a joint project of the University of California, Los Angeles, and the Jet Propulsion Laboratory/California Institute of Technology, funded by the National Aeronautics and Space Administration.

The OGLE project has received funding from the European Research Council under the European Community's Seventh Framework Programme (FP7/2007-2013)/ERC grant agreement no. 246678 to AU. This work has been supported by the Polish Ministry of Science and Higher Education through the program "Ideas Plus" award No. IdP2002 000162 to IS.

## REFERENCES

- Aaronson, M., Mould, J. and Huchra, J. 1980, *ApJ*, **237**, 655.  
 Alard, C. and Lupton, R. H. 1998, *ApJ*, **503**, 325.  
 Arcavi, I. *et al.* 2012, *ApJL*, **756**, L30.

- Assef, R. J. *et al.* 2010, *ApJ*, **713**, 970.
- Assef, R. J. *et al.* 2011, *ApJ*, **728**, 56.
- Blagorodnova, N., Koposov, S. E., Wyrzykowski, Ł., Irwin, M. and Walton, N. A. 2014, *MNRAS*, **442**, 327.
- Bramich, D. M. *et al.* 2008, *MNRAS*, **386**, 887.
- Breiman, L., Last, M. and Rice, J. 2003, *Statistical Challenges in Astronomy*, , 243.
- Campbell, H. *et al.* 2013, *ApJ*, **763**, 88.
- Childress, M. *et al.* 2013, *ApJ*, **770**, 108.
- Drake, A. J. *et al.* 2009, *ApJ*, **696**, 870.
- Drake, A. J. *et al.* 2014, *ApJS*, **213**, 9.
- Fraser, M. *et al.* 2013, *MNRAS*, **433**, 1312.
- Galbany, L. *et al.* 2012, *ApJ*, **755**, 125.
- Gezari, S. *et al.* 2012, *Nature*, **485**, 217.
- Hadjiyska, E. *et al.* 2012, *IAU Symposium*, **285**, 324.
- Hamuy, M. *et al.* 2006, *PASP*, **118**, 266.
- Hubble, E. P. 1926, *ApJ*, **64**, 321.
- Inserra, C. *et al.* 2013, *ATel*, **4863**, 1.
- Kozłowski, S., Kochanek, C. S. and Udalski, A. 2011, *ApJS*, **194**, 22.
- Kozłowski, S. *et al.* 2012, *ApJ*, **746**, 27.
- Kozłowski, S. *et al.* 2013, *Acta Astron.*, **63**, 1.
- Law, N. M. *et al.* 2009, *PASP*, **121**, 1395.
- Maguire, K. *et al.* 2011, *MNRAS*, **418**, 747.
- Marion, G. H. *et al.* 2014, *ATel*, **5891**, 1.
- Mattila, S. *et al.* 2012, *ApJ*, **756**, 111.
- Mowlavi, N. *et al.* 2014, *arXiv*, **1406.7785**, 1.
- Mróz, P. *et al.* 2014, *MNRAS*, **443**, 784.
- Ofek, E. O. *et al.* 2014, *ApJ*, **789**, 104.
- Pan, Y.-C. *et al.* 2014, *MNRAS*, **438**, 1391.
- Peng, C. Y., Ho, L. C., Impey, C. D. and Rix, H.-W. 2002, *AJ*, **124**, 2.
- Perlmutter, S. *et al.* 1999, *ApJ*, **517**, 565.
- Phillips, M. M. 1993, *ApJL*, **413**, L105.
- Pietrukowicz, P. *et al.* 2013, *Acta Astron.*, **63**, 379.
- Planck Collaboration 2013, *ArXiv*, **1303.5076**, .
- Poleski, R., Soszyński, I., Udalski, A., Szymański, M. K., Kubiak, M., Pietrzyński, G., Wyrzykowski, Ł. and Ulaczyk, K. 2011, *Acta Astron.*, **61**, 199.
- Poleski, R. *et al.* 2014, *ApJ*, **782**, 47.
- Poznanski, D. *et al.* 2009, *ApJ*, **694**, 1067.
- Prieto, J. L., Rest, A. and Suntzeff, N. B. 2006, *ApJ*, **647**, 501.
- Quimby, R. M. *et al.* 2011, *Nature*, **474**, 487.
- Rieke, G. H. and Lebofsky, M. J. 1985, *ApJ*, **288**, 618.
- Riess, A. G. *et al.* 1998, *AJ*, **116**, 1009.
- Sako, M. *et al.* 2011, *ApJ*, **738**, 162.
- Schechter, P. L., Mateo, M. and Saha, A. 1993, *PASP*, **105**, 1342.
- Schlafly, E. F. and Finkbeiner, D. P. 2011, *ApJ*, **737**, 103.
- Skowron, J., Wyrzykowski, Ł., Mao, S. and Jaroszyński, M. 2009, *MNRAS*, **393**, 999.
- Smartt, S. *et al.* 2013, *ESO Messenger*, **154**, 50.
- Soszyński, I. *et al.* 2002, *Acta Astron.*, **52**, 143.
- Soszyński, I. *et al.* 2012, *Acta Astron.*, **62**, 219.
- Soszyński, I. *et al.* 2013, *Acta Astron.*, **63**, 21.
- Soszyński, I. *et al.* 2014, *Acta Astron.*, **64**, 1.
- Sullivan, M. *et al.* 2011, *ApJ*, **737**, 102.
- Suzuki, N. *et al.* 2012, *ApJ*, **746**, 85.

- Thöne, C. C., Michałowski, M. J., Leloudas, G., Cox, N. L. J., Fynbo, J. P. U., Sollerman, J., Hjorth, J. and Vreeswijk, P. M. 2009, *ApJ*, **698**, 1307.
- Tylenda, R. *et al.* 2013, *A&A*, **555**, A16.
- Udalski, A. and OGLE III Survey Team 2004, *IAU Circ.*, **8276**, 2.
- Udalski, A., Szymański, M., Kaluzny, J., Kubiak, M., Mateo, M., Krzeminski, W. and Paczynski, B. 1994, *Acta Astron.*, **44**, 227.
- Udalski, A., Kubiak, M. and Szymański, M. 1997, *Acta Astron.*, **47**, 319.
- Udalski, A. *et al.* 2005, *ApJL*, **628**, L109.
- Udalski, A., Szymański, M. K., Soszyński, I. and Poleski, R. 2008a, *Acta Astron.*, **58**, 69.
- Udalski, A., Soszyński, I., Szymański, M.K., Kubiak, M., Pietrzyński, G., Wyrzykowski, Ł., Szewczyk, O., Ulaczyk, K., and Poleski, R. 2008b, *Acta Astron.*, **58**, 89.
- Udalski, A., Soszyński, I., Szymański, M.K., Kubiak, M., Pietrzyński, G., Wyrzykowski, Ł., Szewczyk, O., Ulaczyk, K., and Poleski, R. 2008c, *Acta Astron.*, **58**, 329.
- Udalski, A. 2003, *Acta Astron.*, **53**, 291.
- Udalski, A. 2004, *IAU Circ.*, **8292**, 1.
- Unterborn, C. T. and Ryden, B. S. 2008, *ApJ*, **687**, 976.
- Wozniak, P. R. 2000, *Acta Astron.*, **50**, 421.
- Wright, E. L. *et al.* 2010, *AJ*, **140**, 1868.
- Wyrzykowski, Ł. and Belokurov, V. 2008, *American Institute of Physics Conference Series*, **1082**, 201.
- Wyrzykowski, Ł. and Hodgkin, S. 2012, *IAU Symposium*, **285**, 425.
- Wyrzykowski, Ł. *et al.* 2014, *ArXiv*, **1405.3134**, .